Technical Report No. 32-55

Scientific Experiments for Ranger 1 and 2

jpl
JET PROPULSION LABORATORY
CALIFORNIA INSTITUTE OF TECHNOLOGY
PASADENA, CALIFORNIA

January 3, 1961

NATIONAL AERONAUTICS AND SPACE ADMINISTRATION
CONTRACT NO. NASw-6

Technical Report No. 32-55

Scientific Experiments for Ranger I and 2

JET PROPULSION LABORATORY
CALIFORNIA INSTITUTE OF TECHNOLOGY
PASADENA, CALIFORNIA

January 3, 1961

CONTENTS

TABLES

FIGURES

ABSTRACT

This Report presents descriptions of the scientific experiments to be carried on the *Ranger* 1 and 2 spacecraft. This spacecraft is the first in a series designed for the scientific investigation of the Moon, the planets, and interplanetary space.

Ranger 1 and 2 will carry a family of radiation detectors designed to monitor the intensity of charged-particle radiation. A magnetometer will also be carried to determine the interplanetary magnetic field and its relation to particle flux. Other experiments include a telescope sensitive to Lyman-alpha radiation, a cosmic-dust detector, and scintillation counters to investigate the statistics of solar X-rays.

I. INTRODUCTION

It is the purpose of this document to present the philosophy and plans for *Ranger* 1 and 2, the first in a series of spacecraft designed for the scientific investigation of the Moon, the planets, and interplanetary space. The initial *Ranger* flights will be an effort to perfect the engineering elements of the system. Subsequent space flights will use the same basic *Ranger* spacecraft to carry a capsule to the Moon, and a modified version, to be called *Mariner,* for a near-miss of Venus and for an advanced interplanetary mission.

This Report presents descriptions of the scientific experiments to be carried on the first two *Ranger* spacecraft; however, detailed engineering information on these instruments will be presented in a separate document. This Report, which supersedes a document of the same title,[1] presents the plans for *Ranger* 1 and 2 as of December 1, 1960. Some of the details will, of necessity, be changed as the integration of the instruments into the spacecraft system progresses.

[1]Technical Memorandum No. 33-4.

A. Scientific Objectives

The primary mission of the first two *Ranger* spacecraft is to test the performance of those functions and parts of the spacecraft which are necessary for carrying out subsequent lunar and planetary missions using essentially the same spacecraft design. The secondary mission is the further determination of the nature of the particles and fields in interplanetary space. Special emphasis is given to discovering the mechanisms responsible for the many terrestrial phenomena which appear to be related to solar disturbances. In particular, most of the instruments on *Ranger* 1 and 2 are directed toward the following aspects of solar-terrestrial relationships:

1. Geomagnetic storms and the solar wind. The particles believed to be responsible for geomagnetic storms, the curvature of comet tails, and other phenomena have been directly observed only once (Ref. 1); this single observation was a simple measurement of the flux of positive ions with energies exceeding 15 ev made by *Lunik II*. Thus, the number, energy, and temporal fluctuations are known principally by indirect means, many of which give conflicting results.

2. Replenishing of the outer Van Allen belts by particles of extraterrestrial origin. There exists, at present, some controversy as to the origin of particles in the outer Van Allen belts—whether they are of solar origin or come from the decay of low-energy neutrons created in the Earth's atmosphere by cosmic radiation.

3. Production of high-energy particles by the Sun. The energy spectrum, time variations, and directions of travel of these particles must be determined in order to establish their times, places, and mechanisms of production and storage.

4. Modulation of galactic cosmic rays as observed near the Earth—both the 11-year variation and the shorter-period Forbush decreases. The similarities and differences between these two types of variations are of great importance in determining their mechanisms.

In addition, the data from *Ranger* 1 and 2 should aid in the understanding of those processes occurring at the Sun which give rise to the various particles and modulations seen near the Earth.

For the investigation of these phenomena, the *Ranger* 1 and 2 spacecraft will carry a family of radiation detectors designed to monitor the intensity of charged-particle radiation from energies of about 10 ev to about 100 mev. A summary of the portions of the particle spectrum to be covered by each of the several detectors is given in Fig. 1. The dynamic ranges of these instruments are so chosen that studies can be made of quiet conditions in interplanetary space as well as of the phenomena associated with solar disturbances. A magnetometer for determining the interplanetary magnetic field and its relation to the particle flux will also be carried.

Other scientific experiments on the first two *Ranger* spacecraft are a telescope sensitive to Lyman-alpha radiation for obtaining information on the distribution of neutral hydrogen atoms in the vicinity of Earth, an instrument for the analysis of cosmic-dust particles, and an experiment using a pair of scintillation counters to investigate the statistics of solar X-rays. This last experiment, which is part of the Atomic Energy Commission's *Vela Hotel* project, will not be discussed further in this Report.

A list of these *Ranger* experiments and the cognizant personnel for each experiment is given in the Appendix.

B. Configuration

The basic properties of the spacecraft which will carry the scientific experiments were determined on the basis of the primary mission of performing engineering tests on the spacecraft. One of the most important constraints, in so far as the scientific instruments are concerned, is that the vehicle is attitude stabilized in such a manner that the axis of symmetry (and thus the sensitive surface of the solar panels) points toward the Sun, and the plane which contains this axis and the high-gain antenna also contains the Earth (Fig. 2). The attitude stabilization is a favorable attribute for those experiments which should always point toward either the Sun or the Earth, but it is unfavorable for those experiments which must sample the particle flux from all directions in space.

Most of the scientific instruments are located on a superstructure above the main, hexagonally-shaped body of the spacecraft (Fig. 2). This particular geometry was chosen to satisfy both the low-background magnetic-field requirement of the magnetometer experiment and the requirement that the ionization

chamber be as far removed from the main mass of the spacecraft as feasible.

C. *Trajectory*

The trajectory of the *Ranger* 1 spacecraft is determined from the requirements of both the engineering experiments (which require telemetry contact over a long period of time) and the scientific experiments (which require that a large fraction of this time be spent completely beyond the influence of the Earth and its magnetic field). Furthermore, both the attitude-control system and the Lyman-alpha telescope impose limits on the allowed values of the angle at the spacecraft between the lines to the Sun and to the Earth. The resultant trajectory is an Earth satellite orbit with a nominal 685,000-mi apogee. An isometric view of the trajectory for *Ranger* 1 is given in Fig. 3.

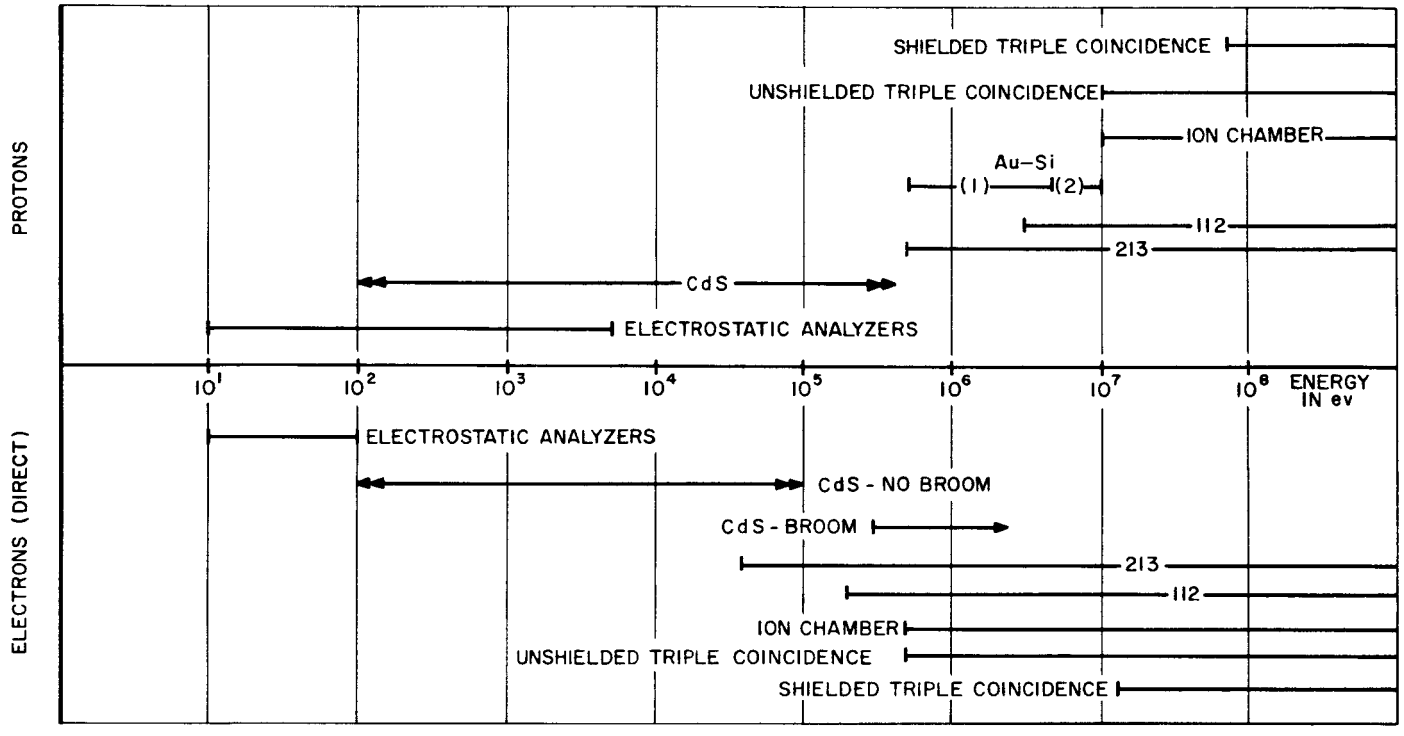

Fig. 1. Energy ranges of radiation detectors for *Ranger* 1 and 2

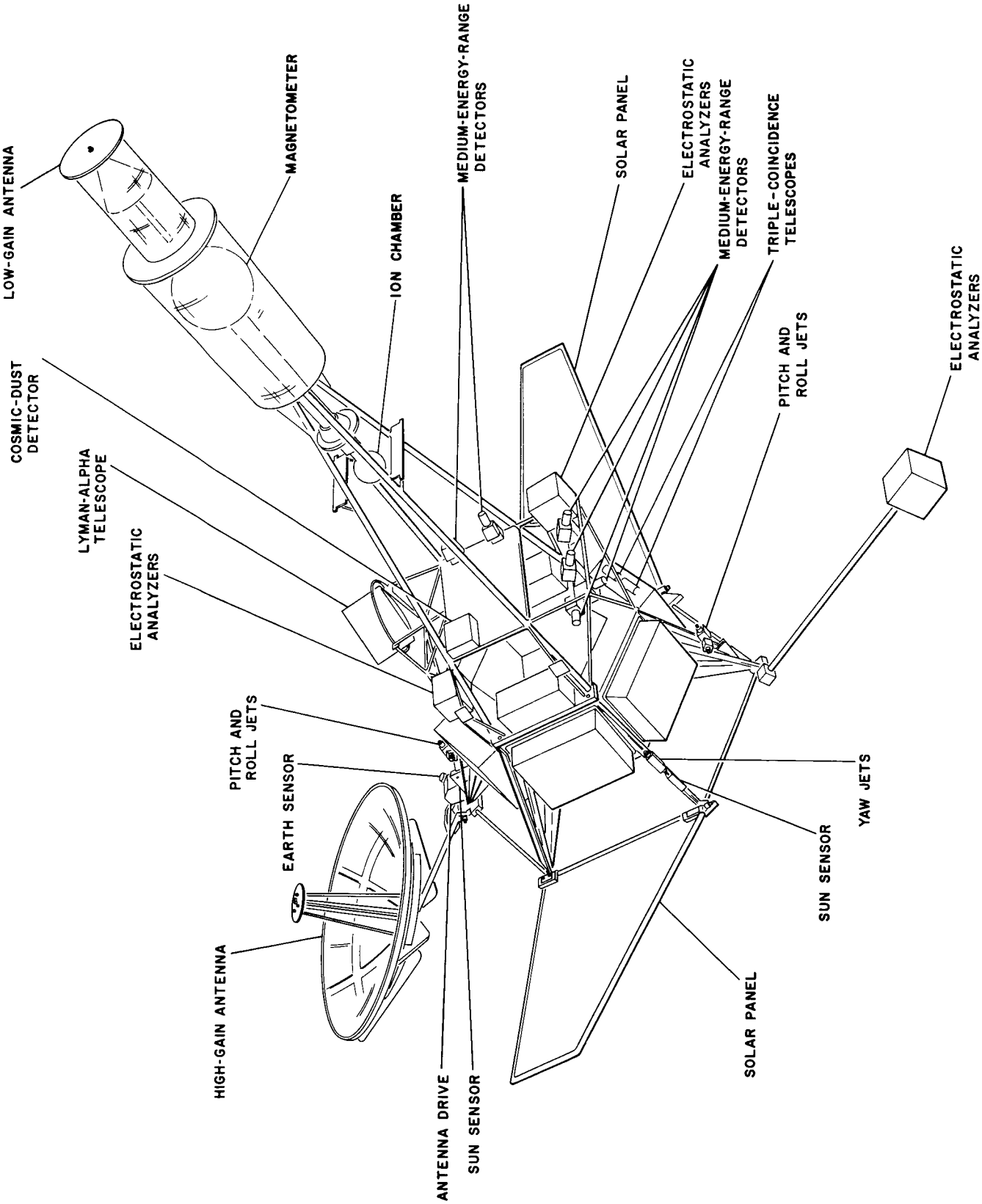

Fig. 2. *Ranger* 1 and 2 spacecraft

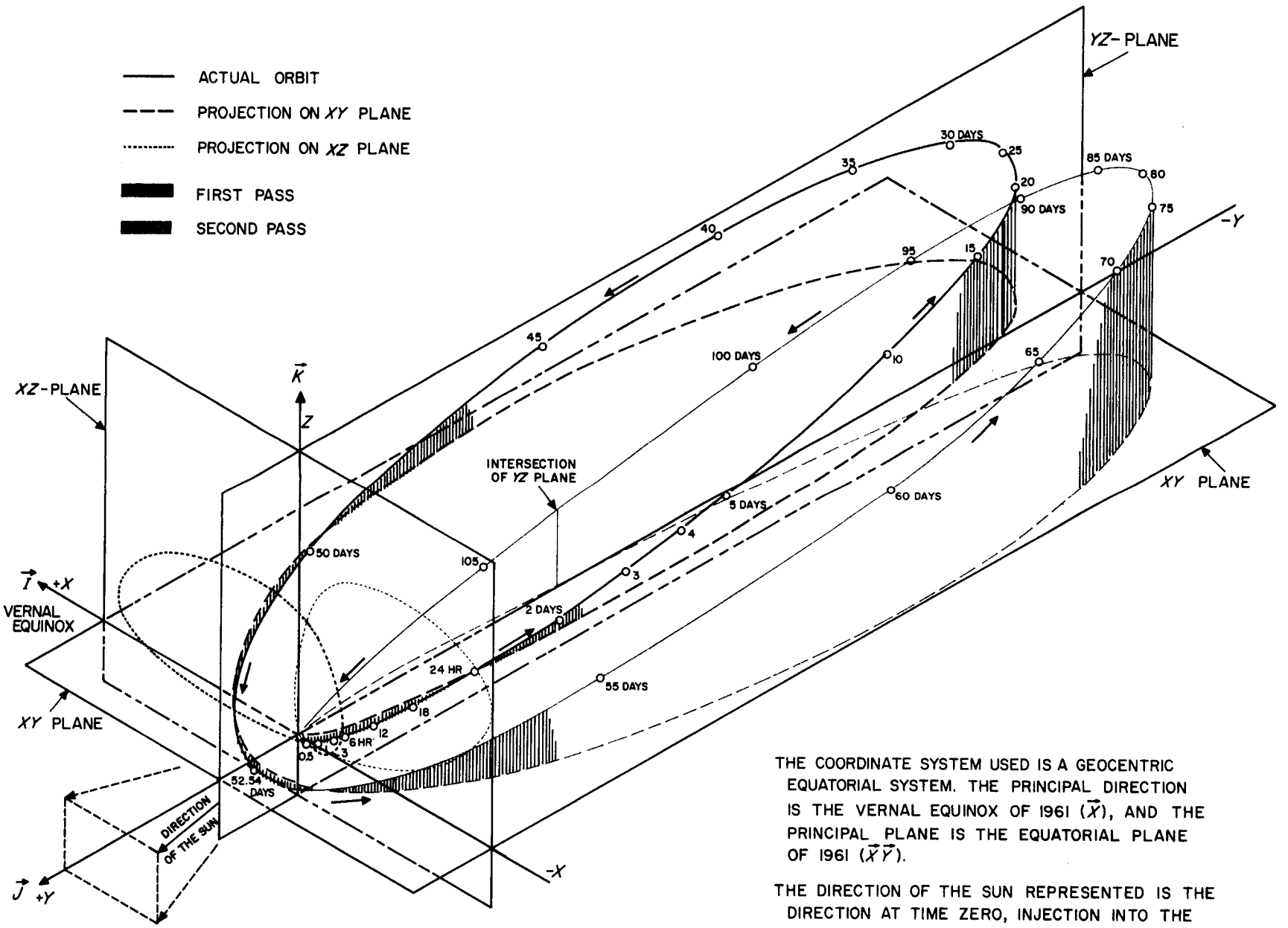

THE COORDINATE SYSTEM USED IS A GEOCENTRIC EQUATORIAL SYSTEM. THE PRINCIPAL DIRECTION IS THE VERNAL EQUINOX OF 1961 ($\vec{X}$), AND THE PRINCIPAL PLANE IS THE EQUATORIAL PLANE OF 1961 ($\vec{X}\vec{Y}$).

THE DIRECTION OF THE SUN REPRESENTED IS THE DIRECTION AT TIME ZERO, INJECTION INTO THE ELLIPTICAL ORBIT.

Fig. 3. Trajectory of *Ranger* 1 spacecraft

II. TRIPLE-COINCIDENCE COSMIC-RAY TELESCOPES

The purpose of the triple-coincidence telescopes is to monitor and to determine some of the properties of the high-energy radiation in interplanetary space. The design and analysis of this experiment, which has the highest threshold energies of the entire complex of radiation detectors on *Ranger* 1, is the responsibility of Drs. C. Y. Fan, P. Meyer, and J. A. Simpson of the University of Chicago.

A. Description of Experiment

Each of the two triple-coincidence telescopes to be carried on *Ranger* 1 and 2 consists of an assembly of seven proportional-counter tubes arranged in the same manner as in the units successfully flown on *Explorer VI* (Ref. 2) and *Pioneer V* (Ref. 3). Six of the seven counters are grouped in a concentric ring around the seventh counter, with the outer counters connected in two adjacent groups of three (see Fig. 4). The pulses from each of the three groups of counters are first amplified and then enter a pulse shaper, which accepts pulses of only a given amplitude or greater and thus acts as a pulse-height discriminator. A standardized pulse is generated and coupled into a triple-coincidence circuit. The outputs of the coincidence circuits and of the center counters alone are then coupled first to scaling stages and, then, after scaling by a factor of 2^5, to the 14-bit counters which are read out by the data-automation system at a rate of once per minute. The maximum counting rate of these counters is such that counting rates up to about 2000 times the normal cosmic-ray background rate can be accommodated.

One of the two telescopes, the high-energy unit, consists of counters whose walls are 0.5-in.-diameter brass tubing, 3 in. in length with a 0.028-in. wall thickness. Lead shielding of 5 gm per cm^2 thickness surrounds this assembly of seven counters. The telescope has a threshold of 75 mev for a triple-coincidence

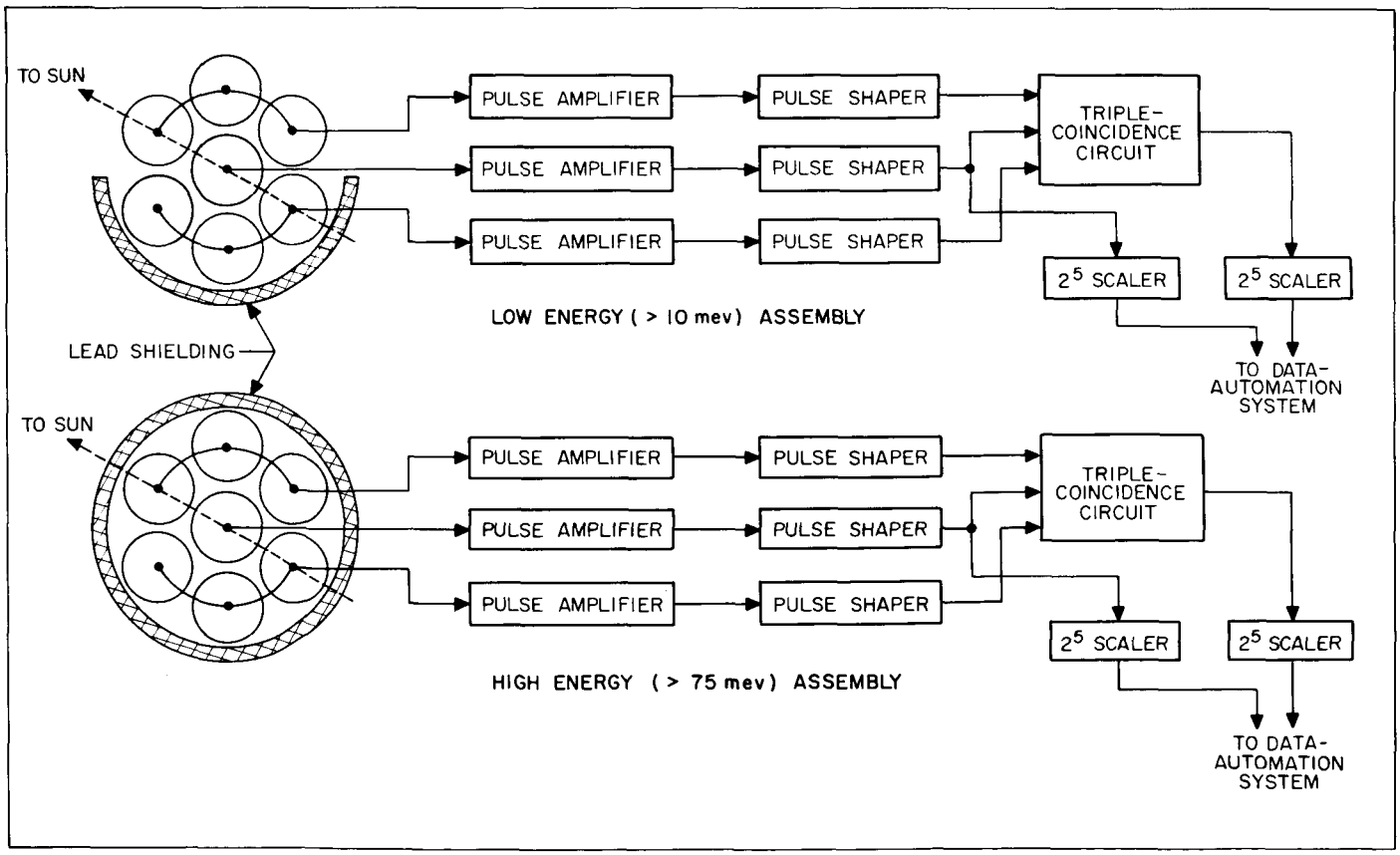

Fig. 4. Triple-coincidence cosmic-ray detector

count due to protons; the corresponding threshold for electrons is 13 mev. The threshold for detection of electrons through their bremsstrahlung radiation is approximately 200 kev. This bremsstrahlung radiation is monitored through the central-tube counting rate rather than by the triple-coincidence counting rate because of the exceedingly low probability that a gamma ray will cause a pulse in each of the three counters. In this manner, a separation of the high-energy-particle radiation from other radiation (gamma rays, electrons between 200 kev and 13 mev, and other charged particles with sufficient energy to penetrate the lead shield plus greater than three but less than five counter-wall thicknesses) can be obtained.

The low-energy telescope has counters with 2.0 ± 0.1 mil steel walls. One half of this assembly has lead shielding (5 gm/cm^2) along the length of the tubes, whereas, the other half of the assembly (the half for which particles can reach the detector without encountering spacecraft structural material) has no shielding. Since particles which encounter any spacecraft structure must also penetrate the lead shielding before detection, the effects of spacecraft material can be neglected here. A knowledge of the counting rates of the high-energy telescope permits the correction of the low-energy-telescope data in order that the particle flux incident on the unshielded portion of the low-energy unit can be calculated. Calculations indicate that a dead angle ϕ, as shown in Fig. 5, will exist for low-energy-particle detection; thus, the actual look angle Ψ for low-energy particles will be not quite 180 deg. The thresholds for triple-coincidence counts by

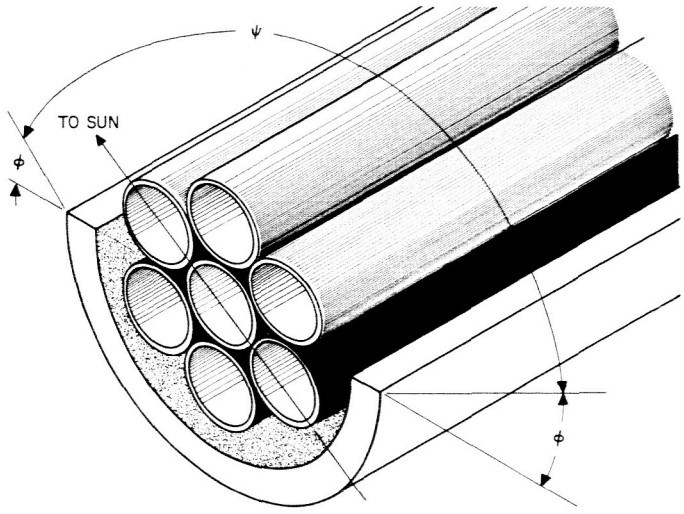

Fig. 5. Low-energy triple-coincidence telescope assembly

particles incident in this angle Ψ are approximately 10 mev for protons and 0.5 mev for electrons.

B. Environment and Spacecraft Integration

The two telescopes are placed with their axes of symmetry on a line which is approximately 1.5 in. above one of the electronics boxes on the main spacecraft. The probe–Sun line is as shown in Figs. 4 and 5; the geometry is such that particles incident from the general direction of the Sun can be seen by the low-energy part of the low-energy telescope as well as by the high-energy telescope.

The total weight of this experiment is 9 lb, and the total power requirement is 500 mw.

III. COSMIC-RAY INTEGRATING IONIZATION CHAMBER

Primary cosmic radiation and other ionizing radiations in the space beyond the Earth's atmosphere will be measured by the quartz-fiber integrating-type ionization chamber developed by H. V. Neher. This type of instrument, which measures the total ionization produced per unit time in a unit volume of standard density air, is simple to operate, maintains a constant calibration for extended periods of time, and also may be accurately calibrated with respect to similar instruments to give an absolute value of the rate of ionization. Because of these characteristics, the ionization-chamber measurement will have the following properties:

1. Intensities measured at different times during a flight of many months may be compared with one another and with other quantities measured during the flight.
2. Intensities measured during the flight of one space probe may be reliably and absolutely compared with those measured by another probe at a different time.
3. The ionization measured in space may be related to ionizations and particle fluxes measured in the Earth's atmosphere and at its surface. This is best accomplished by obtaining absolute values of the ionization in space at the same time that measurements are made at Earth. Realization of this objective may increase greatly the scientific value of all cosmic-ray and related data already accumulated on Earth.

The design and analysis of this experiment is the joint responsibility of the California Institute of Technology (CIT) cosmic-ray group and the Jet Propulsion Laboratory (JPL). Professor H. V. Neher, H. R. Anderson, and W. S. McDonald are the cognizant personnel.

A. Description of Experiment

The ionization chamber consists of a spherical volume of argon gas contained by a thin steel wall and placed near a bulky spacecraft. What is actually measured is the ionization produced in the argon by all naturally occurring (i.e., primary) ionizing particles, that produced by those secondary particles generated in the spacecraft which can penetrate the chamber walls, plus the ionization caused by secondary particles generated in the ion-chamber walls and gas. The relationship between the rate of ionization in the argon and the flux of particles passing through the gas may be written

$$I=\sum_i \int_{4\pi} d\Omega(\hat{r}) \int_0^\infty dE J_i(E,\hat{r}) S_i(E)\rho \qquad (1)$$

where

I = ionization in ion pairs per cm^3 sec in gas of density ρ

ρ = gas density, gm per cm^3

E = kinetic energy of particle, mev

$J_i(E,\hat{r})dEd\Omega$ = flux of type i particles, both primary and secondary, with energy between E and $E + dE$ arriving from solid angle $d\Omega$, units of particles per cm^2 sec

$S_i(E)$ = ions pairs per (gm/cm^2) produced by type i particle with energy E.

It is assumed here that I does not depend upon location within the chamber. Clearly, if I is location-dependent, the ionization chamber gives an average value of I in its filling gas.

The ionization in the volume of argon can be reduced to the ionization in a unit volume of standard air by suitable calibration of the ion chamber. The effect of the wall can also be accounted for since it is thin and has spherical symmetry. Since the effect of the secondary particles produced in the bulk of the spacecraft is difficult to calculate, the ion chamber is located as far as possible from the main bulk of the spacecraft.

Figure 6 shows the ion chamber and its internal mechanism. The entire working mechanism is made of fused quartz, an excellent electrical insulator. The areas which are shown black in Fig. 6 are covered with a conducting coat of aquadag. When no voltage is applied, the fiber, which has a conducting coat, lies about 0.020 in. from the collector. When the power

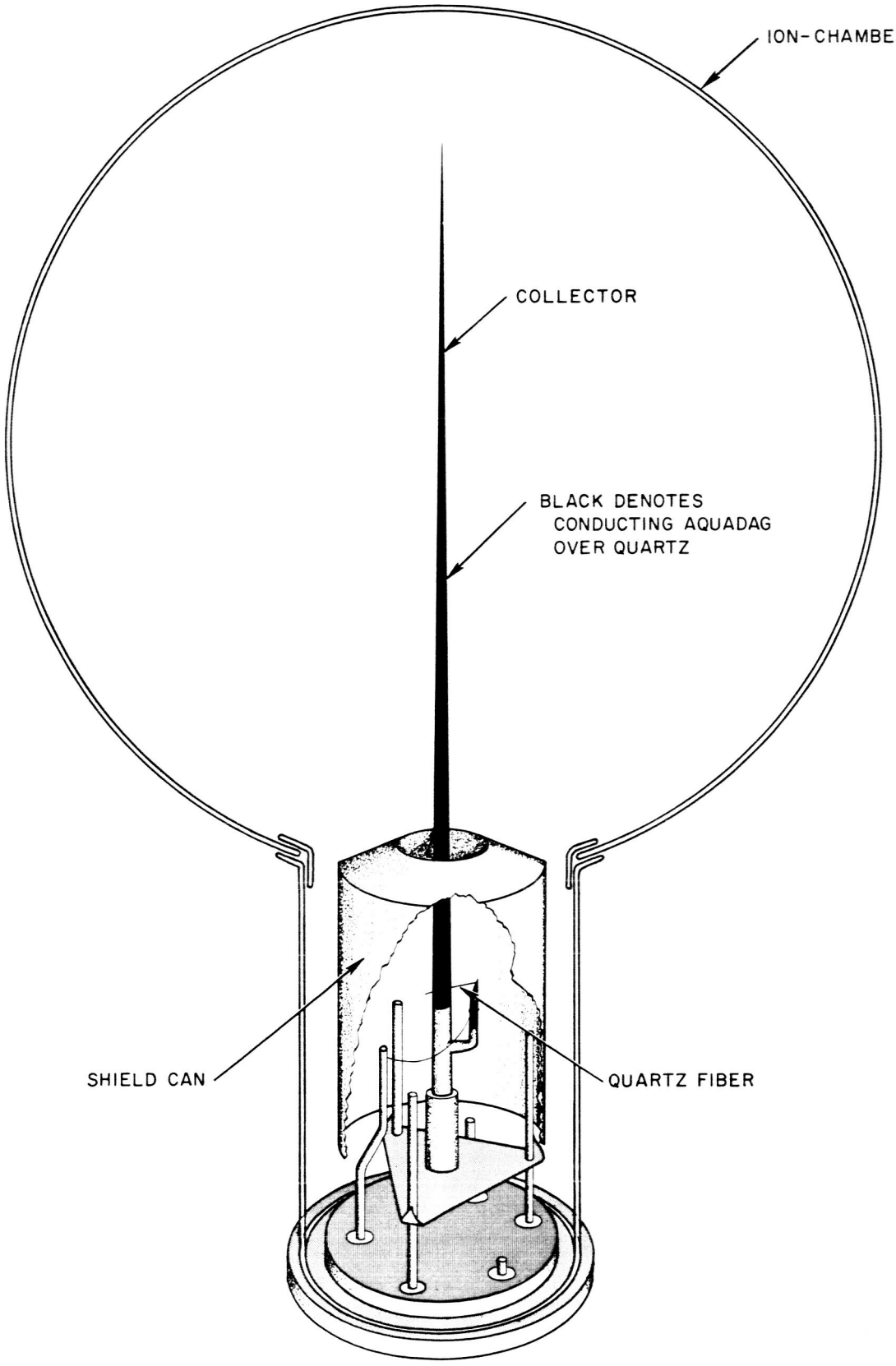

Fig. 6. Cross section of ion chamber and quartz integrating system

is connected, the fiber is bent by electrostatic attraction and touches the collector, charging it to the battery potential. The fiber then moves back to its rest position away from the collector since the fiber, collector, and shield can are all at the same potential.

The electric field between the collector and outer shell is more than sufficient to collect all ions formed in the argon. The ionization current discharges the collector until the fiber again touches and recharges it, simultaneously producing a voltage pulse across a load resistor. Hence, the time between pulses varies inversely with the rate of ionization in the argon; a pulse occurs after about 10^{-10} coulombs have been collected from the argon.

1. Accuracy and Sensitivity to Radiation

The wall thickness determines the minimum-energy particle which can reach the filling gas from the outside. In this case, the thickness has been chosen to match the thickness of the unshielded triple-coincidence proportional-counter telescope made by the University of Chicago. This thickness is ~0.2 gm per cm^2 of stainless steel for the proportional counters and, in the case of the ion chamber, the same total thickness of stainless steel plus copper and silver plating. The minimum-energy particle which can be detected by either of the two instruments is 10 mev for a proton, 40 mev for an alpha particle, and 0.5 mev for an electron, approximately.

Hence, by combining the flux measured by the proportional-counter telescope and the rate of ionization measured by the chamber, some information about the average total specific ionization, $S(E)$ (see Eq.1), of the particles may be obtained. Since S is a function of energy, some information is obtained about the energy of the particles present.

Experience with similar ion chambers made at CIT over a period of years suggests that the ion chambers may be calibrated to within ±1% absolutely and ±0.5% relative to each other, and that they may be expected to hold their calibration to within ±0.5% for many months. The approximate relationship between pulse rate and rate of ionization is shown in Table 1. It is assumed in Table 1 that the chambers are filled with argon at 4-atm pressure and that the quartz systems are similar to those in the *Ranger* 1 proof-test model. The filling pressure may be varied from one instrument to another, with proportional variation in calibration.

As indicated in Table 1, the pulse rate varies linearly with ionization over a wide range. However, the maximum rate at which the chamber can operate is about 100 pulses per sec, and somewhere between 20 and 100 sec^{-1} the response deviates significantly from linearity. Exact calibrations at high rates of ionization will be carried out in the near future.

The steady galactic cosmic-ray ionization is expected to lie between 100 and 1000 ion pairs per cm^3 sec atm of air, depending upon the phase of the 11-year sunspot cycle (Ref. 4). However, bursts of solar particles can produce ionizations of the order of at least 400,000 ion pairs per cm^3sec atm (Refs. 5 and 6). Because there are very few experimental results, this number must be regarded as a lower limit of what may occur. Thus, the pulse rate is expected to be a few pulses per hour most of the time, with occasional increases to 1 pulse per sec or more.

2. Data System

Pulses from the chamber feed to the central data-automation system. A 14-bit word is assigned to this experiment. This word is sampled and transmitted every 28 and 32 sec, alternately. The first 11 bits constitute the ion-chamber pulse register; the last 3 bits constitute the time-count register. Both registers revert to zero after accumulating $(2^{11}-1)$ and (2^3-1) counts, respectively, and neither is ever reset; i.e., reading out or sampling does not change the number in the register. The pulse register counts every ion chamber pulse except during an insignificant 100 μsec dead time while it is being sampled.

The time-count register connects through a switch to a clock which generates a pulse every 4 sec. The switch is turned off when the register is sampled. A pulse from the ion chamber turns the switch on, and succeeding clock pulses are counted until the registers are sampled, at which time the switch is turned off until another chamber pulse occurs. Thus, the data system transmits the time when each pulse occurs to within 4 sec.

Table 1. Pulse rate as a function of ionization

Pulse rate	Ionization	
	Ion pairs/cm^3 sec atm of std air	Roentgen/hr
1/hr	106	1.8×10^{-4}
1/min	6400	0.011
1/sec	384,000	0.66
100/sec	3.8×10^7	66.4

B. Environment and Spacecraft Integration

Ideally, the ion chamber should be located at least 10 or 15 ft from the main mass of the spacecraft in order to reduce the effect of secondary radiation produced in this mass. Because of structural limitations, however, the chamber has been mounted midway between the main spacecraft hexagon and the omnidirectional antenna on the forward structure (Fig. 2). The hexagon subtends about 5% of 4π sterad at this position. Total mass in the hexagon is about 500 lb. In addition, some 15 to 20% of 4π sterad is subtended by superstructure members, the magnetometer, and the omnidirectional antenna, which in general present less absorbing material than does the hexagon.

The complete ion-chamber experiment weighs about 600 gm and requires about 0.01 watts for operation.

IV. MEDIUM-ENERGY-RANGE PARTICLE DETECTORS

The characteristics of the radiation in the energy region from a few kev to a few mev will be measured by a group of relatively small and simple charged-particle detecting modules. It had been planned that the modules would be as nearly identical as possible with regard to voltage requirements, power requirements, output-signal characteristics, telemetry requirements, shape, and method of attachment to the spacecraft. This would permit interchanging of the modules for the yield of the most information for a given flight. Although this plan has proved to be not entirely feasible, the modules are sufficiently similar that it is planned to fly a different combination of these detectors on each of the first two *Ranger* flights.

A. Semiconductor Detectors

A group of charged-particle-detecting modules being developed and constructed by the Department of Physics and Astronomy, State University of Iowa (SUI), has a sensitive element which is a small crystal of photoconductive cadmium sulfide (CdS) approximately 2-mm square and between 0.1- and 0.3-mm thick. The electrical conductivity of such a crystal is proportional to the rate of deposit of energy of ionization in the crystal; hence, if a constant voltage is impressed, the current flow through the crystal can be calibrated in terms of energy flux.

The typical radiation sensitivity of a CdS crystal is 4×10^{-7} amp per unit energy flux (erg/sec-cm^2) for protons, electrons, and X-rays over a wide energy range. The upper limit of this proportional region is the energy required to pass through the CdS crystal (a few hundred kev for electrons and few mev for protons). The lower limit of the region has not been determined accurately, but it is below 100 ev for both protons and electrons. Actually, the sensitivity of most crystals is slightly energy-dependent and may vary by a factor of 2 to 4 for electron energies between 5 kev and 80 kev. The variation, when present, is approximately the same for protons, electrons, and X-rays.

Because of their photoconductivity, these CdS detectors cannot measure low intensities of corpuscular radiation when their axes are closer than 20 deg to the solar vector (35 to 40 deg for the large solid-angle unit). The dynamic range of the detectors is limited at the lower end by a dark current of about 10^{-10} amp; the upper limit is about 5×10^{-5} amp with present circuitry. If the particle flux and the entrance aperture are large enough to give a flux of greater than 10 erg per sec-cm^2 on the crystal, a permanent increase in dark current occurs. It is hoped that the modules will have apertures small enough that this limit will not be reached in passing through the radiation belts of Earth. Modules with larger aperture will have shutters which can be opened after passing beyond the belts. The modules are designed in such a manner that their apertures can easily be modified.

A "magnetic broom", which will deflect low-energy electrons (below about 500 kev) away from the crystal, is incorporated in some of the modules. The magnetic broom is a small permanent magnet; tests have shown that its stray field at the magnetometer in the spacecraft can be kept within acceptable limits (less than 0.5 gamma).

The parts of a CdS detector designed for *Juno II* are shown in Fig. 7. In the lower right-hand corner, the crystal itself, a modified Clairex Type CL-2 photocell, is shown with two leads coming out of it. A series of light baffles are laid out in the adjoining row: the third baffle from the right incorporates the magnetic broom. The modules for the spacecraft incorporate these parts together with the circuitry shown in Fig. 8. The current from a 160-volt supply charges a capacitor through the resistance of the crystal until it reaches the firing potential of a neon bulb across it. The resultant pulses are shaped and fed out to a shift register. The circuit parameters are adjusted in such a manner that the saturation current through the crystal corresponds to about 100 pulses per sec.

B. Geiger Counters

The State University of Iowa is also developing two modules containing Geiger counters. One of these modules uses an Anton 213 end-window counter,

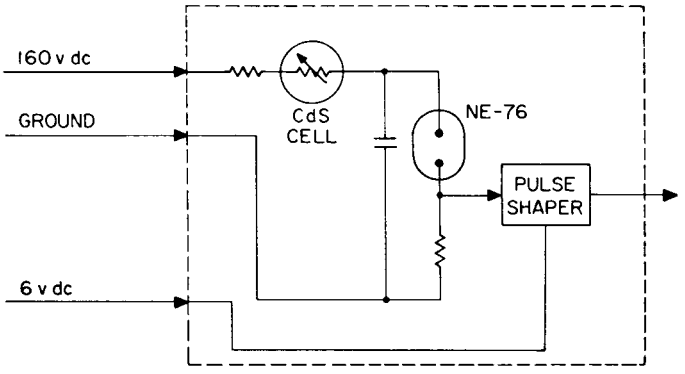

Fig. 8. Circuitry for cadmium sulfide detector

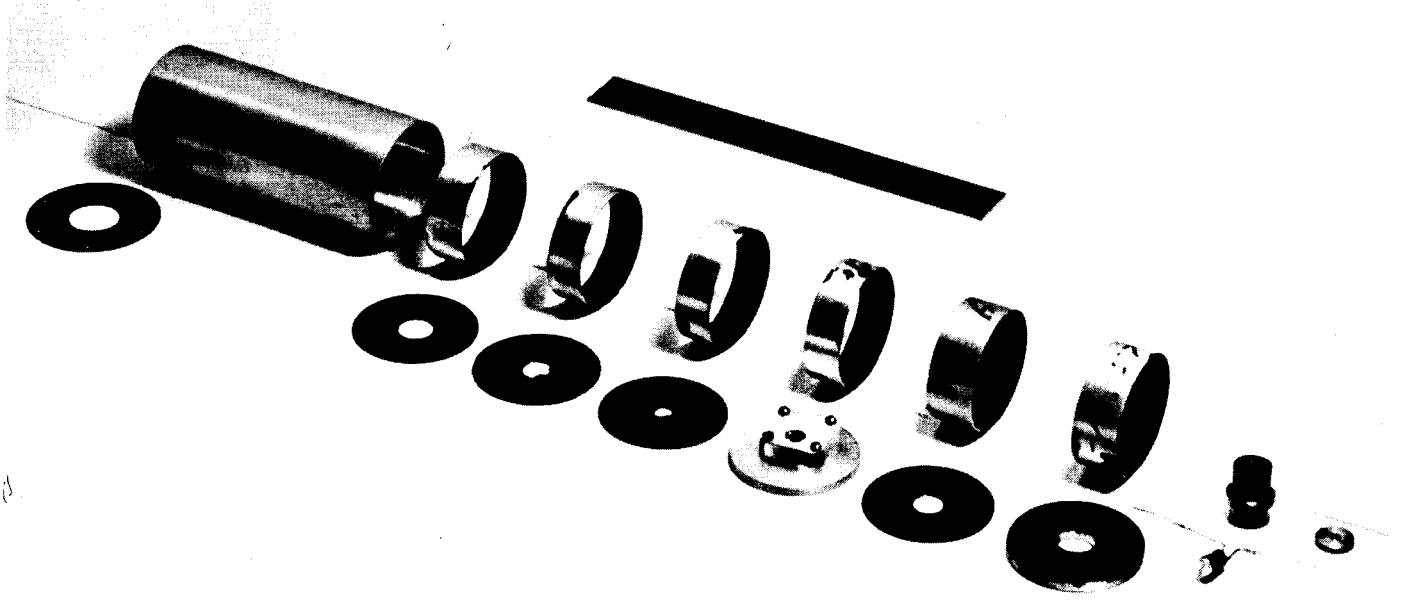

Fig. 7. Cadmium sulfide detector flown on *Juno II*

flown in several successful space probes, which has an effective counting area of approximately 0.12 cm^2 and a 1.2 mg per cm^2 mica window through which can pass electrons above 35 kev or protons above 500 kev. The maximum apparent counting rate of this tube is approximately 20,000 per sec; however, by laboratory calibration, the dynamic range can be extended to over 500,000 counts per sec. The second Geiger-tube module uses an Anton 112 cylindrical thin-wall counter which has a 30 mg per cm^2 titanium wall (corresponding to cut-off energies of 3 mev for protons or 200 kev for electrons). The maximum effective counting area (perpendicular to its axis) of this counter is about 13 cm^2, and its minimum area (parallel to the axis) is about 3 cm^2. Its maximum counting-rate characteristics are similar to those of the 213. Prescaling factors of 2^7 are presently contemplated for both tubes. Figure 9 is a photograph of the two Geiger tubes.

C. *Solid-State Detectors*

The Cosmic-Ray Group at the University of Chicago has developed a module for measuring protons in the energy region from 0.5 to 10 mev; this module incorporates gold-silicon (Au-Si) surface-barrier detectors. The sensitive elements are thin wafers of high-resistivity silicon with a very thin film of gold evaporated on the front surface. A space-charge region (also called the depletion region) extends from the Au-Si interface into the bulk of the silicon. The thickness of this region is adjusted (by adjusting the potential difference across the wafer) to approximate equality with the range of a 2-mev proton. A charged particle incident on the detector will penetrate the thin gold film and produce electron-hole pairs as it passes through the space-charge region. The liberated ion pairs are swiftly swept apart by the high electric field in the space-charge region; this results in a measureable voltage pulse proportional to the amount of energy lost by the particle in passing through the region. An amplifier discrimination level is set in such a way that pulses are produced by protons only if their energy lies between 0.5 and 10 mev; an electron or gamma ray of any energy cannot lose this much energy in so short a distance. It has been found experimentally that the pulse height and shape from the detector for 5.3 mev alpha particles in the presence of an X-ray background flux of about 100 R per hour were essentially unaffected. However, at fluxes near 1000 R per hour, the alpha pulses could not be distinguished from the radiation-induced noise.

The module, a block diagram of which is shown in Fig. 10, contains two Au-Si wafers (approximately

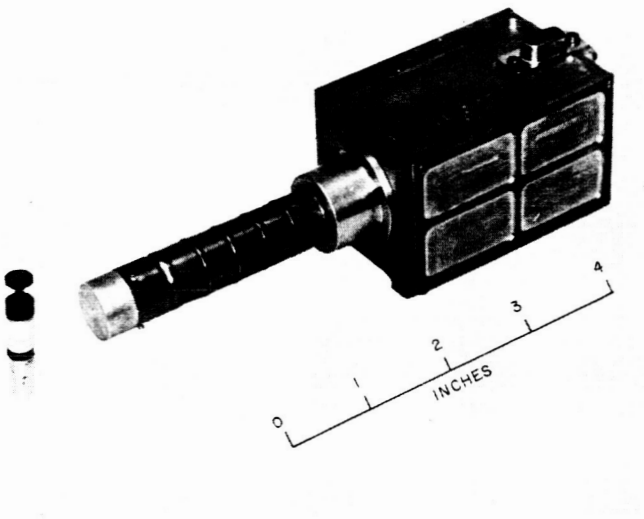

Fig. 9. Anton type 213 (left) and 112 Geiger tubes

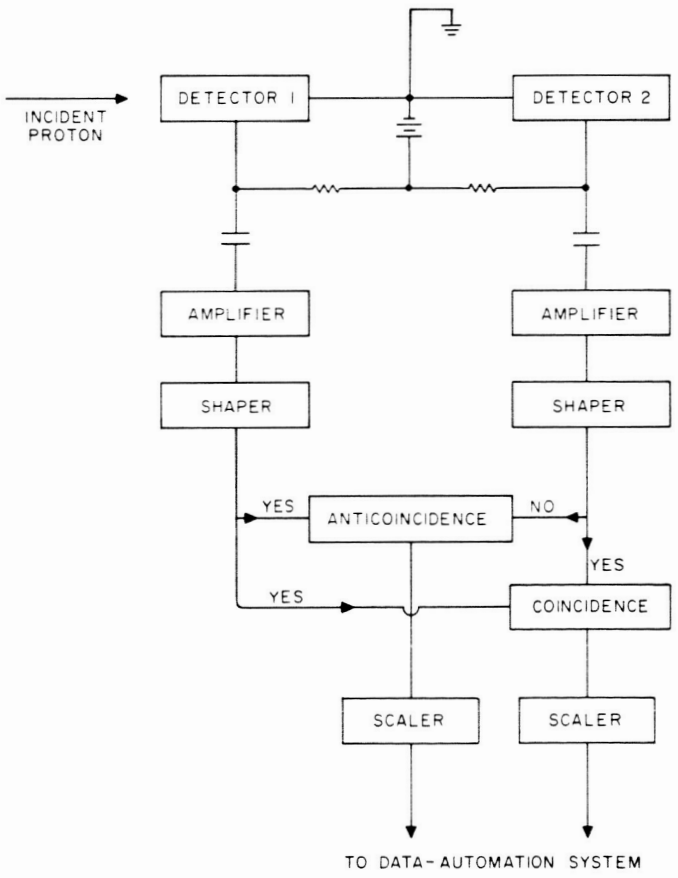

Fig. 10. Block diagram of gold-silicon detector

5 mm diameter and 0.2 mm thick) in a coincidence-anticoincidence scheme. Since a proton must have about 5 mev energy to penetrate completely the first wafer, a coincidence output pulse, which results from a particle triggering both detectors, represents the passage of a proton with energy between 5 and 10 mev. An anticoincidence pulse represents a proton which triggers only the first detector and, hence, has an energy between 0.5 and 5 mev.

Since the detectors are photosensitive, a thin foil ($\sim$¼ mil) of aluminized mylar may be placed above the first detector as a shield against sunlight during the very early portion of the flight before the axis of the vehicle is oriented toward the Sun. The threshold energy for anticoincidence counts would be changed slightly if such a foil were included.

D. System Characteristics

It is possible to carry a total of 6 modules on each flight. The data-automation system (DAS) reads out a 14-bit word once per min from each of the six modules. One of these six shift registers is divided into two 7-bit words to accommodate the Au–Si module (7 bits each for the coincidence and anticoincidence counts) and another is divided into 13-bit and 1-bit words for the CdS module with a removable shutter; the one bit signifies the aperture of the detector.

The six detectors presently planned to be flown on *Ranger* 1 and 2 are listed and their properties are summarized in Table 2. The six *Ranger* 1 modules weigh a total of 3.8 lb and consume approximately 160 mw of power. The *Ranger* 2 modules have essentially the same requirements as for *Ranger* 1.

Table 2. Medium-energy-particle detectors for *Ranger* 1 and 2

Ranger flight	Detector	Angle of axis with probe-Sun line, deg	Angle of axis with ecliptic, deg	Proton energy	Electron energy
1 and 2	CdS with magnet 10^{-2} sterad	45	45	$\geq$400 ev	$\geq$500 kev
1 and 2	CdS 10^{-2} sterad	45	45	$\geq$100 ev	$\geq$100 ev
1 and 2	CdS with shutter 10^{-3} to 5×10^{-2} sterad	45	0	$\geq$100 ev	$\geq$100 ev
1	CdS 10^{-3} sterad	45	0	$\geq$100 ev	$\geq$100 ev
1 and 2	Au–Si	90	90	0.5 to 5 mev 5 to 10 mev	----
1	213 Geiger tube	90	0	$\geq$0.5 mev	$\geq$35 kev
2	112 Geiger tube	0	--	$\geq$3 mev	$\geq$200 kev
2	112 Geiger tube	90	0	$\geq$3 mev	$\geq$200 kev

V. SOLAR-CORPUSCULAR-RADIATION ELECTROSTATIC ANALYZERS

The electrostatic analyzers will measure the low-energy particle flux as a function of charge sign, energy per unit charge, and direction of travel. From the polarity of the deflection-plate voltage, it is known whether electrons or positive ions are being detected at any given time. For the measurement of particle energy, four electron-energy intervals between 13.7 and 110 ev and eight positive-ion-energy intervals between 13.7 and 5490 ev (for singly-charged particles) will be monitored. Direction of travel will be determined by means of six detectors, each with an acceptance angle of approximately 15 deg about the normal direction. These detectors are so situated on the spacecraft that they point in six orthogonal directions—toward and away from the Sun, approximately forward and backward in the ecliptic, and approximately north and south of the ecliptic. The pair of analyzers pointing toward and away from the Sun is located on a boom which, it is hoped, will place the analyzers beyond the plasma sheath of the vehicle itself.

This determination of the direction of travel of the particles, although not extremely detailed, should make it possible to choose among the three principal theoretical models for the interplanetary plasma. These theoretical models are as follows:

1. The particles spiral around the field lines of a solar dipole magnetic field. This theory is consistent with the *Pioneer V* magnetometer data (Ref. 7).

2. The flow away from the Sun is relatively more important than the magnetic effects, and the particles travel, for the most part, radially out from the Sun (Ref. 8). This view is consistent with the observations of the excess curvature of comet tails away from the Sun (Ref. 9).

3. Neither the flow nor the magnetic field is of special importance, and the expansion velocity of the plasma is less than its proton-thermal velocity (Ref. 10).

This JPL experiment is the responsibility of M. Neugebauer and C. W. Snyder as cognizant scientists and C. S. Josias and J. L. Lawrence as cognizant engineers.

The basic properties of the electrostatic analyzers to be carried on *Ranger* 1 can be understood with the aid of Fig. 11. Charged particles entering the instrument are deflected by an electric field which is approximately transverse to the particle velocity. Those particles with a particular charge sign and within a certain range of energy per unit charge and a certain range of angle of incidence are deflected onto the charge collector. Particles which enter the instrument with the wrong charge sign, energy per unit charge, or angle of incidence strike the analyzer walls and are not recorded. The energy distributions of both positively and negatively charged particles entering the device can be determined by varying the sign and magnitude of the deflection voltage.

The circuit used to generate the deflection-plate voltages is composed of a digital sweep generator and a high-voltage amplifier. Table 3 presents the deflection voltages and the energies of singly-charged particles which are most efficiently analyzed at each voltage setting. The spread in particle energy for each deflection-voltage setting is demonstrated in Fig. 13, where the fraction of a beam of singly-charged particles with energy E/E_c normally incident on the analyzer which reaches the collector is plotted vs E/E_c ($E_c = 2.743$ times the deflection voltage = energy required for a constant radius of curvature for normally incident singly-charged particles).

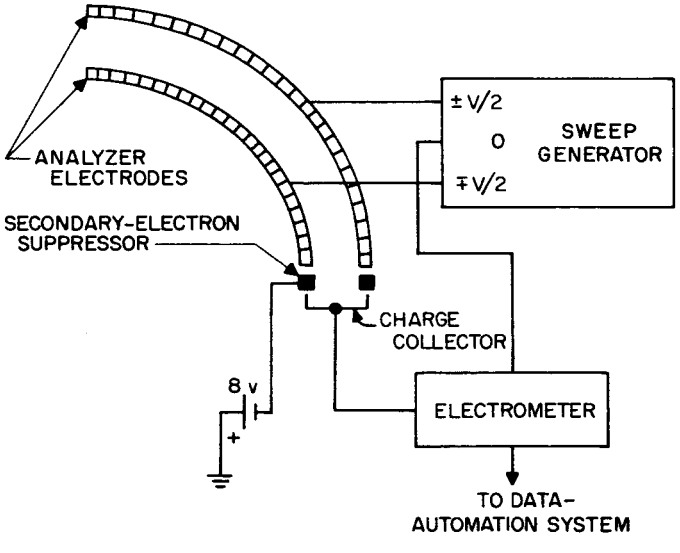

Fig. 11. Solar-corpuscular-radiation instrumentation

The following tabulation gives the sequence of the analyzer operation, which is repeated every 120 sec:

Time in sec	Operation
0 to 9	Deflection voltages are set at step number 1.
8 to 9	The currents to the collectors of all six analyzers are measured.
9 to 18	Deflection voltages are set at step number 2.
.	.
.	.
.	.
108 to 120	Deflection voltages are set back to step number 1. No current readings are taken during this period.

The current-measuring part of the system consists of a dual logarithmic current-to-voltage transducer and a dynamic-capacitor-stabilized carrier-type amplifier. The logarithmic transducer provides bipolar compression over a 7-decade range, thus permitting the detection of both electrons and positive ions without switching or commutation. The instrument can detect currents between 10^{-13} and 10^{-6} amp, which, for the deflection plate geometry being used, corresponds to particle fluxes between 8.6×10^{1} and 8.6×10^{11} cm^{-2} sec^{-1} for each energy interval. The compressed analog output is converted to digital form for transmission accuracy and convenience. The data are presented in the form of 8-bit numbers, and, as the data are the logarithms of the currents measured, the relative accuracy is constant over all 7 decades. The rms current-measuring accuracy of the experiment, based upon the anticipated environment and duration, is expected to be about ¼ of a decade.

Table 3. Electrostatic-analyzer voltage and energy programs

Step number	(Outer—Inner) Deflection-plate voltages, volts	Particle energy, ev	
1	−40	109.7	electrons
2	−20	54.9	
3	−10	27.4	
4	−5	13.7	
5	+5	13.7	protons
6	+10	27.4	
7	+20	54.9	
8	+65	178	
9	+151	414	
10	+365	1000	
11	+840	2300	
12	+2000	5490	

The total weight of the experiment (all 6 units) is approximately 33 lb, and the total power requirement is 2.74 watts. Figure 13 shows photographs of the pair of analyzers which is to point toward and away from the Sun.

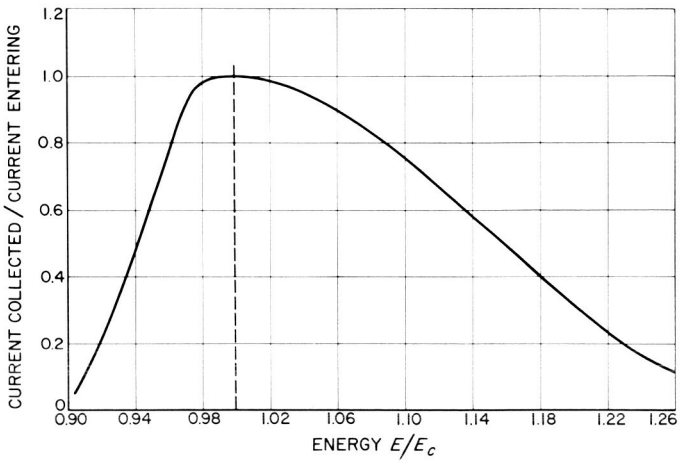

Fig. 12. Experimental energy resolution curve of electrostatic analyzers

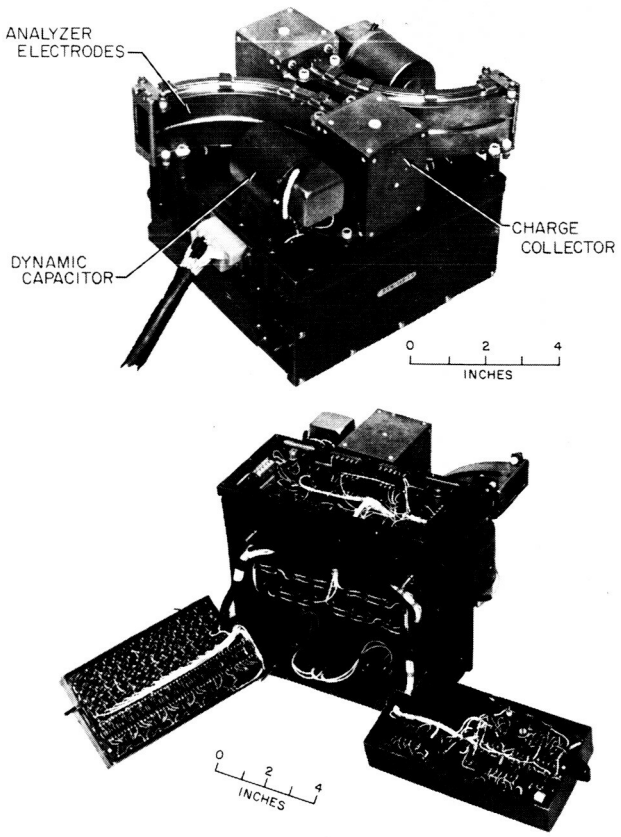

Fig. 13. Pair of electrostatic analyzers

VI. MAGNETOMETER

The prime purpose of a measurement of the interplanetary magnetic field is the determination of its magnitude and direction as well as of the temporal and spatial fluctuations which may occur. There is a strong tendency for any plasma flow from the Sun to drag with it the local solar magnetic field, which, in turn, modifies the flow of the plasma. Futhermore, it is almost certain that the interplanetary magnetic field contributes significantly to the modulation of cosmic rays reaching the solar system from interstellar space, but at the same time this magnetic field allows passage of some solar cosmic rays to the Earth. For a better understanding of the cosmic ray-magnetic field interaction, the correlation of the magnetometer data with the data from the plasma and cosmic-ray experiments, as well as with terrestrial observations of related geophysical phenomena, will be especially enlightening.

Measurements will be made of the geomagnetic field from ~6 Earth radii out in order to obtain additional information concerning the interaction mechanism of the solar plasma with the Earth's magnetic field. These measurements may also give information on the distribution of electric currents in and beyond the outer radiation belts (Ref. 11).

Measurements by the spin-coil magnetometer aboard *Pioneer V* (Ref. 7) have indicated that the average component of the quiescent interplanetary field normal to the spin axis of the vehicle was about 2.5 gammas (1 gamma = 10^{-5} gauss). Considering the distance covered and the resultant change in orientation of the spacecraft's spin axis with respect to radial lines drawn from the Sun, the results are seen to be inconsistent with many models of the interplanetary field. In view of this rather surprising result, it is very desirable that a field measurement be made from a stable platform. Although an investigation into the effect of the interaction of the field of the spinning payload of *Pioneer V* with an assumed ambient plasma has indicated that the effect should be insignificant, it is highly desirable that such a measurement as is planned be made to ensure that this or some other effect is not significant. The instrument to be used for these measurements is an optical pumping magnetometer which is being developed by Varian Associates for Dr. James P. Heppner of the NASA Goddard Space Flight Center.

A. Description of Experiment

On *Ranger* 1 and 2, field measurements to an accuracy of better than 0.05 gamma will be made in the range from 0.05 to 105 gammas. Measurements of fast field fluctuations of up to 30 gammas per sec will also be made in order to study the fine structure of the field. Average vector directions can be computed from the telemetered data.

The alkali vapor used in the present model (see Figs. 14 and 15) is rubidium 87. The relevant energy-

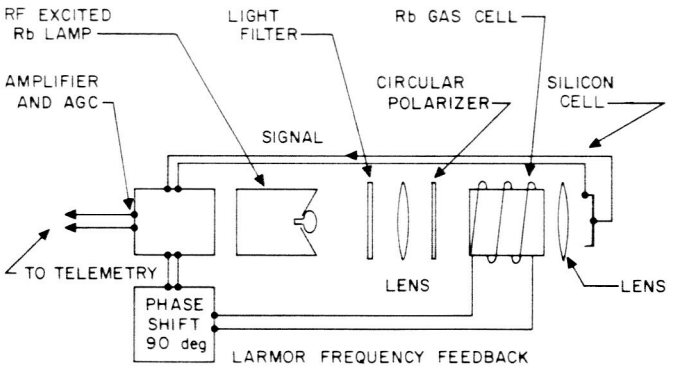

Fig. 14. Rubidium vapor magnetometer

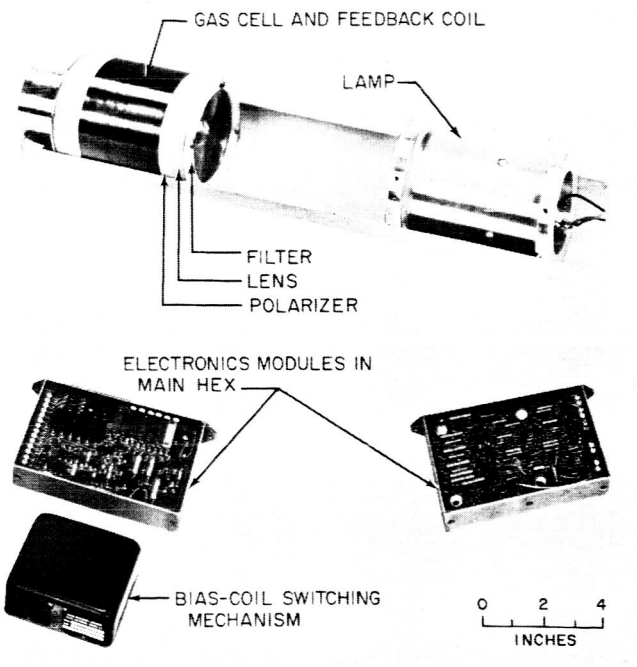

Fig. 15. Components of rubidium vapor magnetometer

level diagram is shown in Fig. 16; each of the hyperfine substates ($F=1$ and $F=2$) is split (Zeeman effect) into $2F+1$ levels in the presence of a magnetic field. The energy difference between adjacent levels with the same F is $h\nu_0$, where ν_0 is the Larmor frequency (6.996 cps per gamma for rubidium 87). The light from the rubidium vapor lamp is filtered and polarized in such a way that only 7947Å right-circularly-polarized light enters the rubidium gas cell. The operation of the magnetometer is most readily understood if the magnetic field is at 45 deg to the propagation vector of the beam and the beam is considered as the superposition of two elliptically-polarized beams having propagation vectors at 90 deg to each other and at 45 deg to the incident-beam direction; each of these component beams can, in turn, be considered as a superposition of right- and left-circularly polarized components, with right-circular polarization dominating. The component beam parallel to the field (in the z direction) is the "pumping" beam; the other (in the x direction) is the "monitoring" beam. The pumping beam causes atoms in the sublevels of the $S_{1/2}$ state to jump to the various sublevels of the $P_{1/2}$

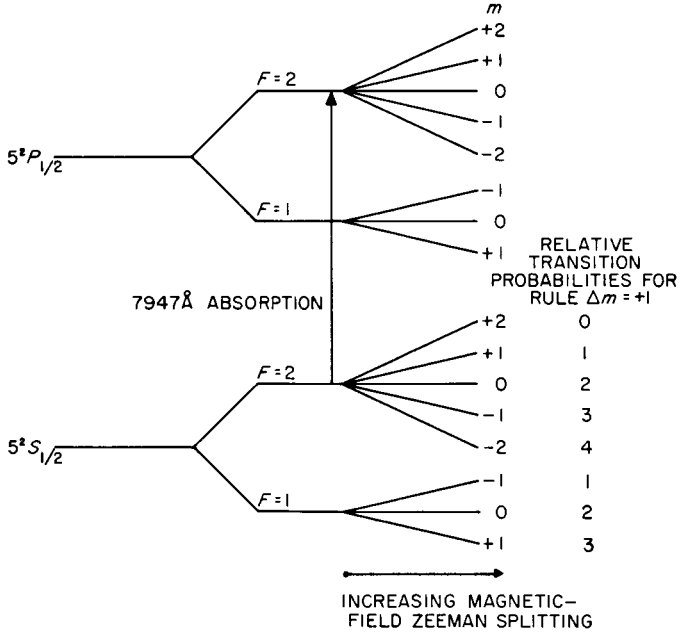

Fig. 16. Energy-level diagram for rubidium 87

state with the selection rule $\Delta m=+1$ for the right-circularly-polarized component and $\Delta m=-1$ for the left-circularly-polarized component. Because a relatively high-pressure gas is present in the cell, the excited atoms in the $P_{1/2}$ state have very short relaxation times for disorientation within the sublevels of this state. Transitions back to the $S_{1/2}$ state occur rapidly with the selection rule $\Delta m=0, \pm 1$ and with all sublevels of the $S_{1/2}$ state having an equal probability of being repopulated. As the process continues, an overpopulation of the $m=+2$ substate of the $S_{1/2}$ state results due to the predominance of right-circularly polarized light, and the sample has a net magnetic moment which precesses about the external magnetic field at the Larmor frequency such that M_z is constant.

However, the magnetic moments of the various atoms in the "pumped" vapor are not precessing coherently (the gas has no M_x), which is a necessary condition before modulation of the monitoring beam can occur. In order to accomplish this, an oscillating field at the Larmor frequency is applied which induces transitions from the $S_{1/2}$, $F=2$, $m=+2$ substate to the $S_{1/2}$, $F=2$, $m=+1$ substate, the transition probability depending on the phase of the precessional motion of the atom. These atoms in the $S_{1/2}$, $F=2$, $m=+1$ substate are now precessing about the field nearly in phase with each other. Since the amount of absorption of the monitoring beam depends on the net M_x of the gas, which now varies sinusoidally at the Larmor frequency, the intensity of the monitoring beam transmitted through the gas cell is modulated at the Larmor frequency. This variation in light intensity is detected with a silicon cell whose signal is amplified, phase-shifted through 90 deg, and inductively applied as positive feedback to the gas cell to maintain the precessional coherency which was started by either a "noise photon" near the Larmor frequency or a spontaneous transition from the $m=+2$ to the $m=+1$ substate of the $S_{1/2}$, $F=2$ level. The frequency of this field-controlled oscillation is the telemetered parameter.

In this instrument, which differs from earlier models in that one light beam is used for both the pumping and the monitoring operation (Ref. 12), a maximum amplitude signal is achieved when the magnetic field is at 45 deg to the light beam (parallel to the pumping beam); there are nodal cones of no response near 0 and 90 deg. In order that field measurements can be obtained for any field direction, bias fields of 10-gamma strength are applied in each of six orthogonal directions consecutively for 10 sec per direction. The bias fields are also required because the limiting value of magnetic field which can be detected by the present model is about 2 gammas. The bias field gives a reference of 10 gammas (chosen for telemetry reasons)

upon which the ambient interplanetary field is superimposed. Since the bias field is known to within 0.01 gammas, the instrument still is capable of accurately measuring very weak magnetic fields. The bias coils are further required in order to obtain the average (over 1 min) direction of the field. Figure 17 shows the exterior of the *Ranger* 1 and 2 magnetometer with the bias coils wound around the 13-in. diameter sphere which surrounds the gas cell.

Because of telemetry restrictions, the frequency range of the *Ranger* 1 and 2 magnetometer is 50 to 800 cps, which corresponds to a maximum detectable total field (interplanetary plus vehicle plus bias coils) of about 105 gammas.

B. Environment and Spacecraft Integration

In order to minimize the magnetic background from the spacecraft and its components, the magnetometer is placed at the extreme front end of the spacecraft, with only the omnidirectional antenna ahead of it. In this configuration, the magnetic sensing element is ~8 ft from the main spacecraft. It is hoped that the background field can be held at less than 0.5 gamma by requiring that every component placed on the payload be magnetically checked and shielded if necessary. It may be that small, highly coercive magnets strategically located on the spacecraft will be required to cancel the spacecraft field at the magnetometer.

The total power requirement for the magnetometer is 4.1 watts, of which 3.66 watts are used for the supply that generates the 100 mc-radio-frequency signal which excites the rubidium lamp. The weight requirement of the sensing head of the magnetometer with associated bias coils, etc., mounted on the superstructure is 3.86 lb. The remaining electronics located in the spacecraft proper totals 1.89 lb.

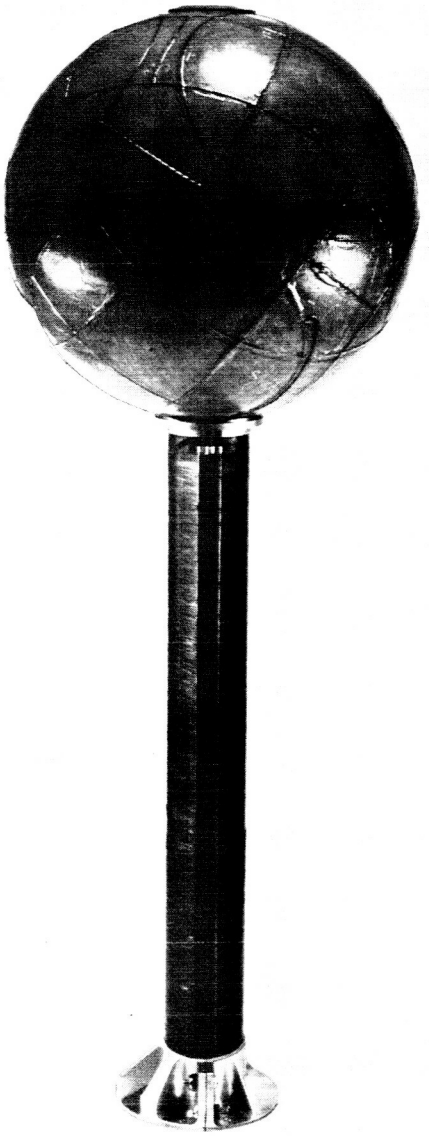

Fig. 17. Rubidium vapor magnetometer with bias coils

VII. LYMAN-ALPHA SCANNING TELESCOPE

The principal purpose of the Lyman-alpha scanning telescope is to obtain a series of low resolution pictures of the Earth and its exosphere in ultraviolet light near the Lyman-alpha wavelength, 1216Å. The source of most of the Lyman-alpha radiation from the vicinity of the Earth is the result of the excitation of neutral hydrogen atoms by either direct or scattered solar Lyman-alpha radiation or by charged particle bombardment. Hydrogen is formed by photo-dissociation of water vapor by sunlight at about 90 km altitude; the hydrogen gas then diffuses outward and is believed to form the main constituent of the exosphere (Ref. 13). Thus, this hydrogen cloud is the last remnant of the Earth's atmosphere and may extend several Earth radii before merging with the gas of interplanetary space or being swept away by a solar wind or radiation pressure.

There is disagreement among interested scientists as to whether or not sufficient hydrogen is concentrated near the Earth to account for the Lyman-alpha radiation in the night sky as observed on high-altitude rocket flights (Ref. 14). One school of thought is that the night-time Lyman-alpha radiation originates through scattering of solar Lyman-alpha radiation by hydrogen atoms in interplanetary space (Refs. 14 through 16). However, Johnson and Fish (Ref. 17) have argued that, if the atoms which scatter the solar Lyman-alpha radiation were in interplanetary space, the orbital velocity of the Earth would produce a Doppler shift which would reduce the reflectivity of the Earth's atmosphere below the value observed on the night-time rocket flight. They also believe that there is very little neutral hydrogen in interplanetary space because either charge exchange with solar-wind protons or the outward radiation pressure on neutral hydrogen atoms by solar Lyman-alpha would sweep the inner solar system clean of neutral hydrogen. By combining the results of the night-time Lyman-alpha observations with the atmospheric temperature and density derived from the *Vanguard I* orbital decay data, Johnson and Fish have constructed a model neutral hydrogen atmosphere. There is some disagreement as to whether or not the Johnson-Fish atmosphere fits the observation of solar Lyman-alpha radiation made on a day-time rocket flight (Ref. 18). The data from the Lyman-alpha telescope and the simultaneous measurement of any solar wind by the electrostatic analyzers and CdS detectors will be of considerable value for the resolution of these problems.

Because of its relatively broad frequency response, the Lyman-alpha telescope can also obtain very valuable information on the geographic extent of any auroral activity which may be occurring during the time of the Earth scan. The Lyman-alpha scanning telescope is being developed for these investigations jointly by the Naval Research Laboratory (T. A. Chubb and R. W. Kreplin) and JPL.

The telescope consists of a parabolic mirror with an ionization chamber located at its focus. A cylindrical radiation shield provides protection against undesirable scattered light and also allows some temperature control. This assembly is mounted in a gimbal system which permits motion of the telescope axis in two perpendicular planes (Figs. 18 and 19).

A. Optics Section

In order to furnish the required optical gain and provide a narrow field of view, a prime-focus telescope

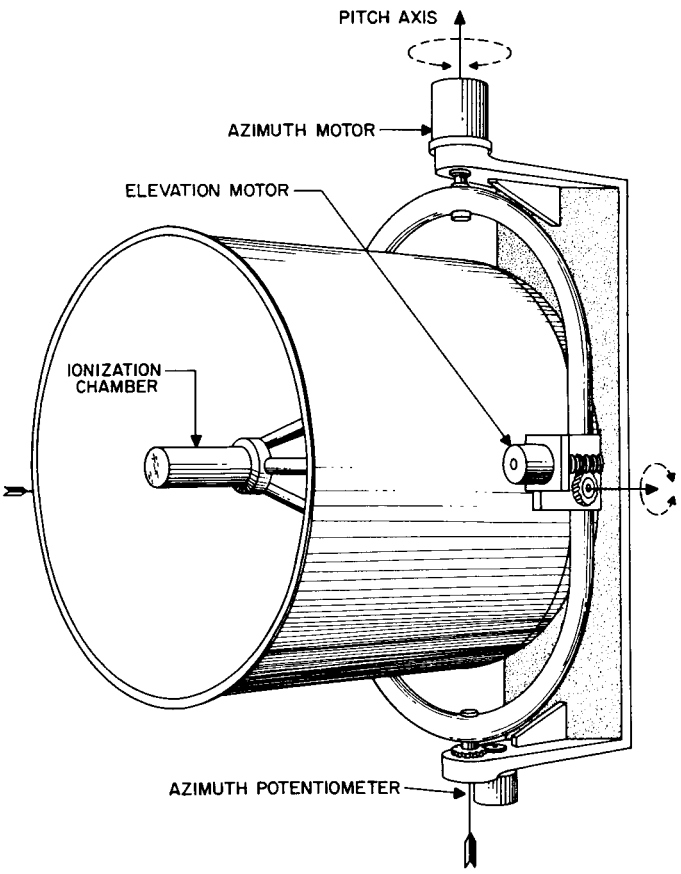

Fig. 18. Lyman-alpha telescope

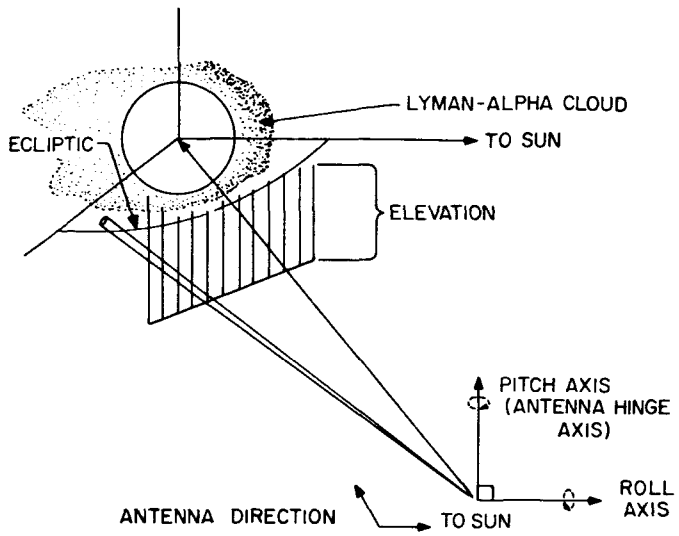

Fig. 19. Scanning raster of Lyman-alpha telescope

is used. The received power P from any sample area is given by

$$P=BA\Omega=\frac{\pi BS}{4F^2} \qquad (2)$$

where

B = effective brightness of source

A = effective collecting area (after correction for obstructions and reflectivity)

Ω = solid angular field of view

S = field stop area

F = effective focal ratio

The mirror is a parabola of 10 in. diameter and $F/0.6$; whereas, the field stop is 0.050 in. diameter. The optical gain is approximately 100 and the field of view is 0.5-deg full-cone angle. The mirror is made of magnesium on which is evaporated first an aluminum layer to provide high reflectance at the Lyman-alpha wavelength and then a MgF_2 coating to prevent oxidation of the aluminum surface. This technique will yield a Lyman-alpha reflectivity between 0.6 and 0.8 while keeping the amount of scattered light to a minimum.

B. Ionization Chamber

The ionization chamber is filled with 15-mm pressure NO gas, which is the active constituent, and 35 mm of a filler gas, CO_2. It is 1 in. in diameter and 1.5 in. long, with a 0.4 in. diameter LiF window cemented with AgCl on one end. The spectral sensitivity of a similar ionization chamber is shown in Fig. 20. The long-wavelength sensitivity cutoff is due to the ionization threshold of NO at about 1350Å; whereas, the short-wavelength cutoff is due to the increasing absorption by the LiF window. The ion-chamber voltage can be adjusted to give the desired gas gain. A typical set of voltages would give gas gains of 1000 and 25, alternately, for which brightness levels between 3×10^{-5} and 1.4×10^{-2} ergs per sec cm^2 sterad and between 1.2×10^{-3} and 0.45 ergs per sec cm^2 sterad, respectively, can be detected without either overloading the amplifier or having a signal which cannot be distinguished from the noise.

C. Scanning Mechanism

The sequence of events for each picture can be described as follows:

1. The telescope moves to a position such that its axis of symmetry points 20 deg away from the center of the Earth in the roll-yaw plane and also in the pitch-yaw plane of the vehicle. This is done by use of the high-gain-antenna position and by a simple position-control servomechanism. The telescope is then switched into its programmed scanning operation.

2. The axis of the telescope sweeps out a raster, as indicated in Fig. 19. Elevation drive is effected by a synchronous motor with the direction of drive determined by two-element commutators. The upper contact reverses the direction of

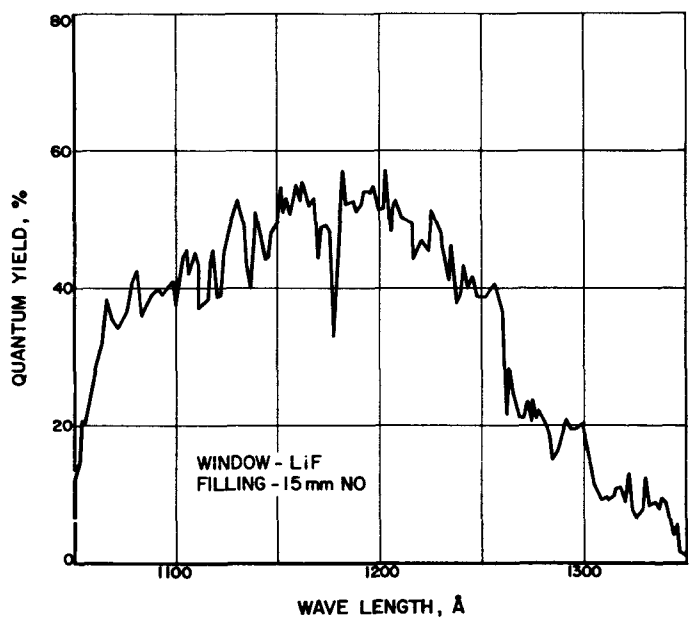

Fig. 20. Spectral sensitivity of Lyman-alpha ion chamber

motion while the lower one initiates the azimuth motor to step out 2 deg in the azimuthal plane. On the completion of this azimuthal motion, the elevation motor is permitted to drive again, the azimuth remaining unchanged, while another line is scanned. During the upward motion of the elevation scan, the gas gain is 25; during the downward motion, it is 1000. The final data are then two series (1 for each gas gain) of 20-strip pictures of brightness versus elevation; each strip is 0.5 deg wide, 40 deg long, and separated from the adjacent strips by 2 deg.

3. After completion of the scanning operation, the telescope remains in its final position and takes background data at gas gain 1000 until the next picture is to be taken. Table 4 presents the program of the series of pictures.

The total weight of this experiment is 14 lb and the total power requirement is 1.15 watts.

Table 4. Program of Lyman-alpha scanning operations

Picture number	Distance from Earth at time of picture, Earth radii	Linear size of picture, Earth radii
1	8.9	±3.3
2	11.0	4.0
3	12.9	4.7
4	14.6	5.3
5	16.2	5.9
6	17.7	6.4
7	21.3	7.8
8	27.9	10.2
9	37.6	13.7
10	67.4	24.5
11	99.2	36.1
12	130	47.4
13	153	55.6
14	174	63.3
15	183	66.5

VIII. COSMIC-DUST DETECTORS

In addition to the current interest generated by the possible damage effects (Refs. 19 and 20) of cosmic dust particles, there is considerable interest in the properties of these particles because their source is not yet completely understood. A knowledge of the source and dynamics of the interplanetary dust particles would lead to a better understanding of the history and evolution of the solar system. There are four postulates as to the source of the interplanetary solid matter:

1. The disintegration of comets. Particles which are cometary debris may have very low densities; i.e., from 0.05 to 1 gm per cm^3.
2. The collisional fragmentation of planetoids. Such bodies may resemble meteorites found on Earth. Stony meteorites have densities of about 3.5, whereas iron meteorites have densities of about 7.8 gm per cm^3.
3. A fossil accumulation from the early days of the solar system.
4. Interstellar particles which do not belong to the solar system.

For dust particles with masses of less than 1 gm, the theory of cometary origin is currently the most popular because of observations of the interaction

with the Earth's atmosphere of particles with masses estimated to be between 10^{-6} and 1 gm (Refs. 21 and 22). However, all the large meteoritic bodies which have been recovered on the Earth's surface are of the planetary type. The mass at which a division between the two types occurs (if there is such a division) is still open to question. It is believed very unlikely that many of the smaller particles in interplanetary space have been there for the life of the solar system (Ref. 23). Small particles, for which the outward force due to solar radiation is greater than the inward force due to solar gravity, are removed from the solar system very rapidly. Larger particles spiral into the Sun as a result of the Poynting-Robertson effect. At least 99% of all meteors (particles which have an observable interaction with the Earth's atmosphere) have, when they reach the Earth, velocities below what they would have required if they had come from outside the solar system (Ref. 24). However, the velocity distribution is not known for the smaller particles; some of them may indeed come from interstellar space.

The cosmic-dust experiment on *Ranger* 1 and 2 is the design of a group at Goddard Space Flight Center under the direction of W. M. Alexander.

A. Detectors

The experiment is designed to measure the flux of dust particles in interplanetary space as a function of the particles' energy, momentum, and direction of incidence. From these data, something can be determined about the dust number-density, the effect of the Earth's gravitational field on the density distribution, the mass and velocity distributions of the dust particles, the distribution of their orbits in space, and any time variations of these properties which may exist.

The composite dust-detection instrument consists of a light-flash impact detector which is sensitive to the light emission occurring during dust-particle impacts on an exposed surface and another impact sensor which is a crystal transducer attached to the same exposed surface.

1. Light-Flash Impact Detector

The light-flash detector is a ruggedized, low-noise, scintillator-type photomultiplier with an aluminum-compound layer, about one-thousand angstroms thick, evaporated onto the window to shield the photosensitive cathode from ambient extraneous light from the Sun, Earth, and Moon. The response of this unit is believed to be approximately proportional to the kinetic energy of the impacting particle (Ref. 25). The threshold of detectability is expected to correspond to the impact of a particle with 10^{-2} ergs of kinetic energy. Pulses from the photomultiplier excite three current-sensitive amplifiers which are driven from separate dynodes. The pulse rate of the first (least-gain, highest-energy impacts) of these three amplifiers is recorded in a counter of two binaries. The second amplifier excites a counter of three binaries, and the last excites a counter of five binaries. At the end of each minute, all these counters are read and reset; thus the data are presented as three-channel (integral) pulse-height analysis with a multiplicative factor of 31.6 among the sensitivities corresponding to adjacent channels. It is possible to record 3 high-energy impacts, 7 medium- plus high-energy impacts, or 31 total above-threshold-energy impacts per minute without overflow of any of the counters.

2. Crystal Transducer Impact Detector

The crystal transducer is essentially a microphone coupled to the photomultiplier tube in such a way that potentials are generated by the crystal on collision of a particle with the exposed surface of the photomultiplier tube. The crystal response is believed to be related to the component of the impacting particle's momentum perpendicular to the impact surface (Refs. 26 and 27). The threshold of detectability of the crystal detector is approximately 10^{-4} dyne-sec.

The crystal output excites a parallel resonance voltage-sensitive amplifier with a mid-frequency bandpass of 100 kc and an over-all gain of 100 db. The pulse rate from this amplifier is recorded in a counter of two binaries. A second counter of two binaries receives its excitation from a point in the amplifier of 20 db less gain. Thus, the data from this detector, which is also read once per minute, are presented as a two-channel analysis with a capacity of 3 high-momentum impacts or 3 above-threshold impacts per minute without overflow of either of the counters.

The complete calibration of any system of cosmic-dust detection depends on the availability of a hypervelocity micro-particle in the laboratory; such particles with well-known mass and velocity are not yet available with velocities above about 10 km per sec. However, progress is being made in this field, and such particles may be available within the next year.

As a check on the stability and aging of the detectors, a simple in-flight calibration of the photomultiplier and the electronics will be performed as follows: after the binaries have been read and reset, a calibration pulse is fed into the first microphone amplifier and to a neon bulb mounted on the photomultiplier tube. The preset amplitude of the calibration pulse is just sufficient to trigger all of the first binaries in each counter. Therefore, any decrease in sensitivity can be detected by an apparent drop in flux of one high-energy, high-momentum particle per minute accompanied by the apparent increase in flux of one medium-energy and/or one low-momentum particle per minute.

If, for the present, it is assumed that the theoretical threshold sensitivities given in the preceding paragraphs correspond to the actual thresholds, that the light-flash detector response is directly proportional to the particle's kinetic energy, and that the microphone response is directly proportional to the particle's momentum, then the experimental data can be used to determine the particle mass and velocity distributions, as shown in Fig. 21. In this diagram, the line AB represents the threshold sensitivity for the low-energy channel of the light-flash detector; all velocity-mass points to the right of this line represent a particle with sufficient kinetic energy to give a count in this channel. Similarly, the lines CD and EF represent the higher sensitivity thresholds. All velocity-mass points to the right of the line IJ represent particles with sufficient momentum to register in the least-sensitive counter of the crystal microphone, and those to the right of the line GH correspond to the most sensitive microphone channel. Thus, each impact can be represented by a point in one or another of the eleven odd-shaped boxes shown in Fig. 21. The number of points in box 9 relative to the number of points in boxes 5, 10, and 11 may give some information about the mass-density (and thus about the source) of very small particles. This is possible because the mass corresponding to the arrow marked $\rho = 0.1$ is the smallest mass particle of density 0.1 gm per cm^3 which will not be rapidly blown out of the solar system by radiation pressure. Unless either the momentum detector actually can go to lower momentum values or the energy-detector thresholds are higher than is presently indicated, it will not be possible to differentiate among particles above or below the parabolic limit (dividing velocity between particles which do and do not belong to the solar system) with this experiment.

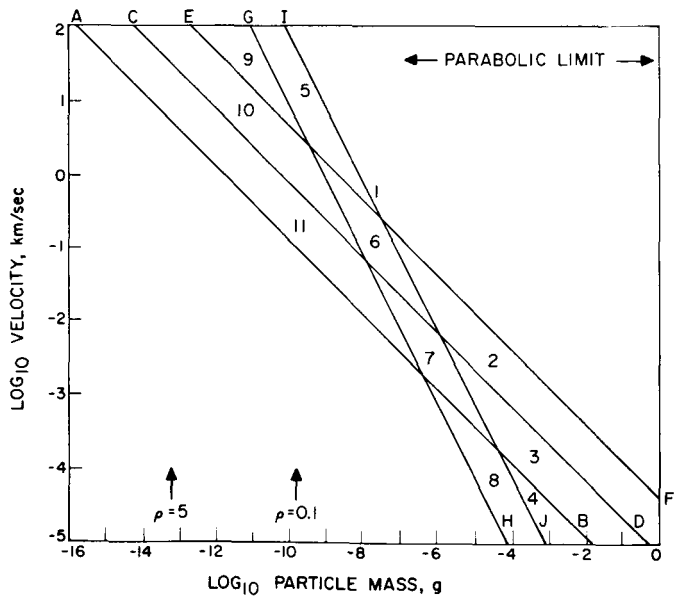

Fig. 21. Cosmic-dust detector velocity–mass diagram

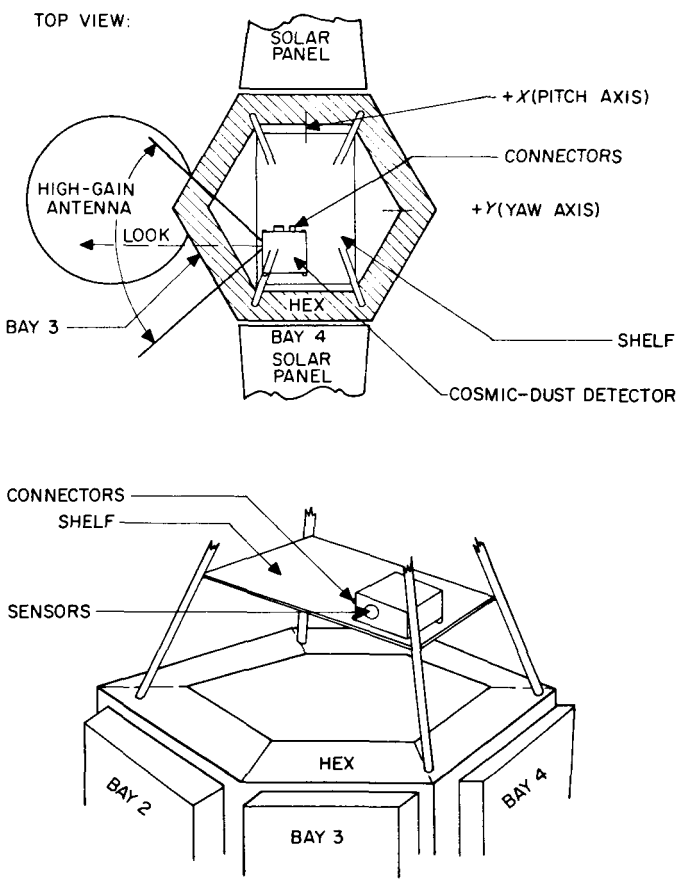

Fig. 22. Location of cosmic-dust detectors on *Ranger* 1 and 2 spacecraft

B. Environment and Spacecraft Integration

The composite package is mounted in such a way that the normal to its sensitive surface (1.25 in. diameter circle) lies in the plane defined by the probe-Sun and the probe-Earth lines and is perpendicular to the probe-Sun line on the side of the vehicle toward Earth (see Fig. 22). With such an arrangement, the detector will point to the West in the ecliptic for about the first 30 days and then to the East in the ecliptic for about the next 20 days. Thus, both forward- and retrograde-motion particles can be detected. The total weight of this experiment is 3.55 lb, and the total power requirement is 0.20 watts.

IX. DATA-AUTOMATION SYSTEM

A data-automation system (DAS) is required in order to prepare the data coming from the several experiments for acceptance by the telemetry system. In general, this preparation may involve such functions as programming, encoding, storage, and a general direction of the flow of the data.

Figure 23 shows the specific functions of the *Ranger* 1 and 2 data-automation system. The DAS receives information from the particle detectors and the 400-cps master clock and supplies control pulses to the electrostatic analyzers and the magnetometer. There are three binary outputs of the DAS corresponding to three scientific-data telemetry channels.

To understand the basic operation of this DAS is simply to realize that its basic function is one of commutation among the various sensors. Other operations performed by the DAS are a parity check on each data word, the denotation of the time of occurrence of pulses from the ion chamber, and the analog-to-digital conversion of the electrostatic-analyzer data. Certain of the experiments are commutated as 14-bit words; whereas others are commutated as 8-bit words in 3-word groups, which requires relatively complex decommutation equipment.

The decommutation equipment is being designed to provide synchronization of the spacecraft data, to reconstruct the data, and to decode and to print (or punch on tape) the information in decimal form.

The DAS flight article has a weight of 13 lb and consumes 1.023 watts maximum power. The system was developed utilizing as many "off-the-shelf" items with conventional circuitry as possible in order to minimize design problems and satisfy schedule requirements.

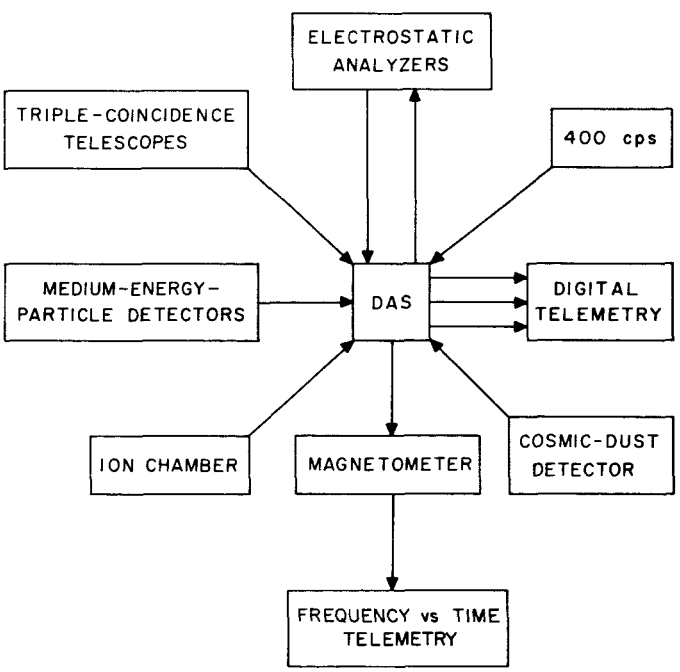

Fig. 23. Scientific data-automation system for *Ranger* 1 and 2

X. DATA REDUCTION AND PRESENTATION

The data-handling system to be used in connection with the *Ranger* program is of particular interest because it is the first time that preparation has been made for the handling and analyzing of scientific data prior to the carrying out of such a complex space experiment. In the past, it appeared sufficient to concentrate all efforts on the launching of the vehicle. As a result, in the subsequent analysis of the data, those responsible for this analysis were forced to disregard approximately 95% of the information received. The difficulty resulted, for the most part, from the fact that data were not in a convenient, usable form.

The system to be used for the data handling of the *Ranger* series of experiments utilizes an IBM 7090 high-speed automatic digital computer as the major information-transforming device. This computer is capable of performing 250,000 arithmetical or logical operations each second.

The *Ranger* spacecraft will transmit its data in both analog and digital form. Each mode will require special ground equipment to effect the transformation of data to a form suitable for the computer. Specifically, the Lyman-alpha data will be in analog form and the magnetometer data will be in the form of frequency versus time; all other data will be received in digital form as encoded by the data-automation system described in Sec. IX.

The data will be received by the Deep-Space Instrumentation Facility (DSIF), which is comprised of antennas at Goldstone, California; Woomera, Australia; and in the area of Krugersdorp, Union of South Africa.

The data will be recorded on magnetic tapes at each antenna site, and these tapes will then be transported to the JPL telemetry Data Reduction Laboratory (faster teletype transmission will also be used), where the signals will be demodulated from the carrier frequency and the noise will be removed. Also, the magnetometer frequency data and the Lyman-alpha analog data will be transformed into digital data for each 0.1 or 0.01 sec period. All digitized data will then be transformed by a specially built data translator and recorded on a magnetic tape that can be fed directly into the computer.

In order to correlate the data with the position of the vehicle, those parameters which give the initial trajectory conditions will be fed into the system. When used in conjunction with the trajectory computer program, these parameters give the desired positions at any time.

The computer accepts this information serially into its memory. The first operation is to check the data to determine whether or not they pass certain parity tests and frame-synchronization markers inherent as check points in the transmitted data. Such tests will not be passed if noise has so distorted the data that a "one" appears as a "zero", or vice versa, since all of the digital data are in binary form. The expected strength of the signal is such that, at the threshold distance of 1 million mi, on the average, all but 1 binary digit per 1000 would be discernible. Once it is established that the data are correct, calibration factors are applied to each experiment in order that the numbers will be of significance to the reader. Since many of the experiments use counters which accumulate information rather than reset each time, the computer calculates successive differences between readings and also calculates averages, ratios, and other desired parameters. The computer also makes comparisons with the results of other experiments.

An output format is created which labels each experiment and gives the time the data were received in the spacecraft. It is in this capacity that presentation for useful interpretation by the scientific community becomes important. All of the transformed data will be printed numerically on the IBM tabulator, which prints 120 digits per line and 8 lines per in. (1 line generally represents 1 min. worth of data). Approximately 6 pages laid side by side will be necessary to represent 1 line for 1 minute. It would still be very difficult to examine visually these large amounts of numbers with the immediate hope of establishing any trends within any single experiment or to compare one experiment with any of the other experiments. Therefore, it is valuable to convert a pertinent number of the columns of printed data into a graphical form using an x, y plotter with time along the base at a rate of 1 hour per in. Several experiments can then be plotted above each other such that it is much easier to see any correlation and trend with time among the various experiments, relevant geophysical data, and terrestrial observations of solar events which will be noted on the same plots. From these observations, it should be possible to deduce a mathematical model which can be placed into the computer for testing.

REFERENCES

1. Gringhauz, K. I., Bezrukikh, V. V., Ozerov, V. D., and Rybchinski, R. E., "A Study of the Interplanetary Ionized Gas, High Energy Electrons and Solar Corpuscular Radiation using Three-Electrode Charged-Particle Traps Installed on the Second Soviet Cosmic Rocket," *Physics Express*, 2 (10): 29-31, July 1960.

2. Fan, C. Y., Meyer, P., and Simpson, J. A., "Cosmic Radiation Intensity Decreases Observed at the Earth and in the Nearby Planetary Medium," *Physical Review Letters*, 4: 421-423, 1960. See also: Fan, C. Y., Meyer, P., and Simpson, J. A., "Trapped and Cosmic Radiation Measurements from *Explorer VI*," pp. 951-966, *Proceedings of First International Space Science Symposium* (Edited by H. Kallman Bijl). North Holland Publishing Company, Amsterdam, 1960.

3. Fan, C. Y., Meyer, P., and Simpson, J. A., "Preliminary Results from the Space Probe *Pioneer V*," *Journal of Geophysical Research*, 65: 1982-1983, 1960.

4. Neher, H. V., "The Primary Cosmic Radiation," *Annual Review of Nuclear Science*, 8: 217-242, 1958.

5. Rothwell, P., and McIlwain, C., "Satellite Observations of Solar Cosmic Rays," *Nature*, 184: 138-140, July 18, 1959.

6. Anderson, K. A., et al, "Observations of Low-Energy Solar Cosmic Rays from the Flare of 22 August 1958," *Journal of Geophysical Research*, 64: 1133-1147, 1959.

7. Coleman, P. J., Jr., Davis, L., and Sonett, C. P., "Steady Component of the Interplanetary Magnetic Field: *Pioneer V*," *Physical Review Letters*, 5: 43-46, 1960.

8. Parker, E. N., "Dynamics of the Interplanetary Gas and Magnetic Fields," *Astrophysical Journal*, 128: 664-676, 1958. See also: Parker, E. N., "The Hydrodynamic Treatment of the Expanding Solar Corona," *Astrophysical Journal*, 132: 175-183, 1960.

9. Bierman, L., "Solar Corpuscular Radiation and the Interplanetary Gas," *Observatory*, 107: 109-110, 1957. See also: Bierman, L., "Physical Processes in Comet Tails and their Relation to Solar Activity," *Mémoires de la société royale des sciences de Liège*, 13 (Series 4): 291-301, 1953.

10. Chamberlain, J. W., "Interplanetary Gas. II. Expansion of a Model Solar Corona," *Astrophysical Journal*, 131: 47-56, 1960.

11. Smith, E. J., Coleman, P. J., Jr., Judge, D. L., and Sonett, C. P., "Characteristics of the Extraterrestrial Current System: *Explorer VI* and *Pioneer V*," *Journal of Geophysical Research*, 65: 1858-1861, 1960.

12. Bell, W. E., and Bloom, A. L., "Optical Detection of Magnetic Resonance in Alkali Metal Vapor," *Physical Review*, 107: 1559-1565, 1957.

13. Johnson, F. S., "The Exosphere and Upper F Region," *Journal of Geophysical Research*, 65: 2571-2575, 1960.

14. Kupperian, J. E., Jr., Byram, E. T., Chubb, T. A., and Friedman, H., "Far Ultraviolet Radiation in the Night Sky," *Planetary and Space Science*, 1: 3-6, 1959.

15. Struve, O., "Far-Ultraviolet Radiation of the Night Sky," *Sky and Telescope*, 17: 445-448, 1958.

16. Shklovsky, I. S., "On Hydrogen Emission in the Night Glow," *Planetary and Space Science*, 1: 63-65, 1959.

17. Johnson, F. S., and Fish, R. A., "The Telluric Hydrogen Corona," *Astrophysical Journal*, 131: 502-515, 1960.

18. Purcell, J. D., and Tousey, R., "The Profile of Solar Hydrogen-Lyman-α" *Journal of Geophysical Research*, 65: 370-372, 1960.

19. Whipple, F. L., "The Meteoritic Risk to Space Vehicles," *Vistas in Astronautics*, Volume I (Edited by M. Alperin and M. Stern). Pergamon Press, New York, 1958.

20. Bjork, R. L., and Gazley, C., Jr., *Estimated Damage to Space Vehicles by Meteoroids*, Research Memorandum RM-2332. RAND Corporation, Santa Monica, California, February 20, 1959.

21. Jacchia, L. G., "The Physical Theory of Meteors. VIII. Fragmentation as Cause of the Faint-Meteor Anomaly," *Astrophysical Journal*, 121:521-527, 1955.

22. Whipple, F. L., and Hawkins, G. S., "Meteors," *Encyclopedia of Physics*, 52: 519-564, 1959.

23. Wyatt, S. P., and Whipple, F. L., "The Poynting-Robertson Effect on Meteor Orbits," *Astrophysical Journal*, 111: 134-141, 1950.

24. Whipple, F. L., "Photographic meteor orbits and their distribution in space," *Astronomical Journal*, 59: 201-217, 1954.

REFERENCES (Cont'd)

25. Alexander, W. M., Private Communication

26. Alexander, W. M., et al., *Calibration of a Rocket-Borne Micrometeorite Detection System*, Research Foundation Report, Oklahoma State University, April 1957.

27. Cohen, H. A., Corman, A. and Dubin, M., "Calibration of Micrometeoritic Detectors Used in Satellites and Rockets," *Proceedings of Third Symposium on Hypervelocity*, Chicago, Armour Research Foundation of Illinois Institute of Technology, October 7-9, 1958, Vol. 1: 405-424, February 1959.

APPENDIX

Jet Propulsion Laboratory, Division of the Space Sciences, Cognizant Personnel for *Ranger* 1 and 2

DIVISION PROGRAM REPRESENTATIVE: M. Eimer
PROJECT ENGINEER: R. L. Heacock
PROJECT SCIENTIST: M. Neugebauer

Experiment	Sponsoring Agency/Experimenter(s)	JPL Cognizant Scientist	JPL Cognizant Engineer
Triple-Coincidence Telescopes	University of Chicago/C. Y. Fan, P. Meyer, and J. A. Simpson	M. Neugebauer	J. D. Allen
Integrating Ionization Chamber	California Institute of Technology and JPL/H. V. Neher and H. R. Anderson	H. R. Anderson W. S. McDonald	H. R. Anderson W. S. McDonald
Medium-Energy Particle Detectors		C. W. Snyder	J. D. Allen
(a)Geiger Tubes and CdS Detectors	(a)State University of Iowa/J. A. Van Allen		
(b)Au-Si Detectors	(b)University of Chicago/C. Y. Fan, P. Meyer, and J. A. Simpson		
Electrostatic Analyzers	JPL/M. Neugebauer and C. W. Snyder	M. Neugebauer C. W. Snyder	C. S. Josias J. L. Lawrence
Magnetometer	NASA Goddard Space Flight Center/J. P. Heppner	D. E. Jones	M. B. Gumpel
Lyman-Alpha Telescope	Naval Research Laboratory and JPL/T. A. Chubb, and R. W. Kreplin	H. T. Bull	D. D. LaPorte
Cosmic-Dust Detectors	NASA Goddard Space Flight Center/W. M. Alexander	M. Neugebauer	E. S. McMillan
Data System	JPL	R. Nathan	W. E. Brown, Jr.
Ground Support Equipment	JPL	—	G. F. Baker